FRACTURE CONDUCTIVITY OF THE EAGLE FORD SHALE

A Thesis

by

JAMES J. GUZEK

Submitted to the Office of Graduate and Professional Studies of
Texas A&M University
in partial fulfillment of the requirements for the degree of

MASTER OF SCIENCE

Chair of Committee,	A. Daniel Hill
Committee Members,	Ding Zhu
	Michael Pope
Head of Department,	A. Daniel Hill

August 2014

Major Subject: Petroleum Engineering

ABSTRACT

Hydraulic fracturing is a well completions technique that induces a network of flow channels in a reservoir. These channels are characterized by fracture conductivity, a measure of how easily a liquid or gas flows through the fracture. Fracture conductivity is influenced by several variables including fracture surface roughness, fracture closure stress, proppant size, and proppant concentration. The proppant concentration within a fracture can significantly affect the magnitude of fracture conductivity, which enhances the productivity of a hydraulically fractured well. Therefore, understanding the relationship between proppant concentration and fracture conductivity is critical to the successful development of unconventional reservoirs such as the Eagle Ford Shale.

This work investigates the fracture conductivities of seven Eagle Ford Shale samples collected from an outcrop of facies B. Rough fractures were induced in the samples and laboratory experiments that closely followed the API RP-61 procedure were conducted on the samples to measure the unpropped and propped conductivities. Propped experiments were performed with 30/50 mesh white sand at two different areal concentrations within the fracture, 0.1 lb/ft^2 and 0.2 lb/ft^2. Assuming a cubical packing arrangement, the proppant pack is calculated to be a partial monolayer of 0.8 layers at 0.1 lb/ft^2 and a pack of 1.6 layers at 0.2 lb/ft^2.

The results show that when the fractures are propped with 0.1 lb/ft^2 or 0.2 lb/ft^2, fracture conductivity values are approximately two orders of magnitude greater than unpropped conductivity values. Therefore, even low areal concentrations of proppant in a fracture can significantly enhance conductivity in the Eagle Ford Shale. Comparing

the results of the two propped experiment types, conductivity values at 0.1 lb/ft^2 proppant concentration are on average 49% higher than conductivity values at 0.2 lb/ft^2. This difference is attributed to the partial monolayer pack at 0.1 lb/ft^2 and proppant pack of 1.6 layers at 0.2 lb/ft^2. However as closure stress increases from 1,000 psi to 6,000 psi, fracture conductivity at 0.2 lb/ft^2 decreases more slowly than conductivity at 0.1 lb/ft^2. These results suggest that the conductivity of the denser proppant pack at 0.2 lb/ft^2 is more resistant to the flow inhibiting effects caused by proppant embedment and proppant crushing.

DEDICATION

I would like to dedicate this work to my loving parents, John and Suzanne, and to my brothers, Daniel and John, who encouraged and supported me throughout the course of my graduate studies.

ACKNOWLEDGEMENTS

I would like to thank Dr. Daniel Hill and Dr. Ding Zhu for inviting me to join and study in their petroleum engineering graduate program. Their guidance and support helped me complete this study.

I would also like to thank Dr. Michael Pope for giving me the opportunity to make a journey to West Texas in order to collect the Eagle Ford shale samples used in this study. I would like to thank John Maldonado, Zhang Junjing, Anton Kamenov, Kathryn Briggs, and Timothy Jansen for their contributions to the project.

I would like to thank the Crisman Institute for their financial support. I would like to thank Elligton Geologic Company for performing the mineral analysis.

I would finally like to thank the Harold Vance Department of Petroleum Engineering for providing me with the education and training necessary to begin a career in petroleum engineering. Your generosity is much appreciated.

NOMENCLATURE

A	Cross-sectional area (in^2)
hf	Fracture height (in)
kf	Facture permeability (md)
L	Length over pressure drop (in)
M	Molecular mass (kg/ kg mole)
p_1	Upstream pressure (psi)
p_2	Downstream pressure (psi)
R	Universal gas constant (J/mol K)
T	Temperature (K)
v	Fluid velocity (ft/min)
W	Mass flow rate (kg/min)
z	Gas compressibility factor (dimensionless)
ρ	Fluid density (lbm/ft^3)
μ	Fluid viscosity (cp)
Δp	Differential pressure over the fracture length (psi)
P_{cell}	Average cell pressure within the fracture
$k_f w_f$	Fracture conductivity (mD-ft)

TABLE OF CONTENTS

Page

LIST OF FIGURES

Page

LIST OF TABLES

Page

1. INTRODUCTION

1.1 Hydraulic fracturing of unconventional reservoirs

Shale reservoirs are characterized by ultra-low matrix permeability, which causes hydrocarbons to be trapped in localized pore spaces and obstructs their flow to the wellbore. Hydraulic fracturing is one stimulation technique that boosts the transmissibility of reservoir fluids by creating a network of flow channels in the formation. By increasing reservoir communicability to the wellbore, oil and gas recovery can be increased to economically profitable levels.

A hydraulic fracturing treatment opens flow channels in the reservoir by pumping proppant-laden fluid at high rates and pressures into a formation. During the treatment the fluid's pressure is increased to levels exceeding the rock strength and confining stress, inducing a progressive network of cracks from the wellbore into the formation. The fracturing fluid also acts as a conduit for proppant transport; while the fractures are held open during the treatment by the fracturing fluid pressure, the fluid deposits the fine-mesh sand or ceramic particles in the fractures. After the pumping operation has ceased, the created fractures begin to close due to overburden pressure on the reservoir. However, the proppant counteracts the reservoir's compressive stresses and maintains fracture width, sustaining flow long after the treatment.

Fracture conductivity is a measure of a gas or liquid's ability to flow through a fracture. It is the product of fracture permeability and fracture width, and is directly related to the production capacity of the well (Economides et al., 2012). Fracture conductivity is influenced by several variables including fracture surface roughness,

fracture closure stress, proppant size, proppant concentration, and rock geomechanical properties. Therefore, optimizing conductivity by tailoring a well's fracturing treatment to local reservoir characteristics is important to the oil and gas industry for economic reasons.

The roots of hydraulic fracturing can be traced back to alternative stimulation methods used in the United States during the mid-1860's, an era when Civil War Col. Edward Roberts patented the technique of "shooting" shallow oil wells with nitroglycerine torpedoes. During the 1930's, operators began pumping acid down the wellbore as a stimulation method; the corrosive liquid enhanced production by fracturing the formation and permanently etching flow channels into fracture surfaces. From these acid treatments, a relationship between treating pressure and formation breakdown was recognized by Floyd Farris of Stanolind Oil and Gas Corporation. Based on Farris' studies, Stanolind pumped the first "Hydrafrac" treatment using 1,000 gallons of a fluid composed of gasoline, naphthenic acid, and palm oil in a Kansas gas well in 1947 (Montgomery et al., 2010).

During the 1950's, oil-based fracturing fluids were eclipsed by water-based "slickwater" fluids composed of low concentrations of guar gum and sand. Slickwater treatments offered a lower cost and greater safety profile than oil-based fluids. During the late 1960's, the industry determined that greater long-term production from wells could be achieved by pumping much larger volumes of fluid and sand; this change brought about the widespread replacement of slickwater treatments with massive crosslinked gel treatments carrying high proppant concentrations into the formation

(Brannon et al., 2004). However, it was not until the late 1980's that crosslinked treatments were identified to cause greater than 80% damage to fracture permeability due to the gel residue retained in the proppant pack during flowback. This recognition incentivized many operators to return to slickwater fluids during the 1990's (Brannon et al., 2004).

During the mid-1990's, several operators tested slickwater frac treatments containing friction reducer and 0.5 lbs./gal sand concentration in gas wells in the East Texas Cotton Valley Sandstone formation and the Barnett Shale. The production results showed that slickwater treatments provided the "same inferior stimulation" as crosslinked treatments in the two tight gas reservoirs, but at up to a 60 % reduction in fracturing costs (Mayerhoff et al., 1997) ; (Walker et al., 1998). Several researchers theorized that the benefits of the slickwater treatments were caused by factors including a partial monolayer proppant pack in the fractures and the absence of gel damage to the proppant pack. Therefore, the slickwater treatments were thought to result in higher effective fracture widths than crosslinked treatments as a result of these factors (Palisch et al., 2008) ; (Mayerhoff et al., 1997). By 1997, advances in horizontal drilling and multistage fracturing treatments employing high-rate slickwater fluids initiated the exploration of other shale plays.

Development of the Eagle Ford Shale began in October 2008 when Petrohawk Energy Corporation substantiated the economic profitability of the field with the results of its first horizontal well. Using experience from the Barnett Shale, operators initially

treated Eagle Ford wells with slickwater treatments, but got lower than expected production rates in the liquid hydrocarbon region (Mullen et al., 2010).

Subsequent analysis of offset well data determined that the Eagle Ford Shale is more ductile than Barnett Shale and more susceptible to proppant embedment (Stegent et al., 2010). Based on developments in the Bakken shale, during 2009 operators returned to both crosslinked fracturing treatments carrying higher proppant concentrations and hybrid treatments, in which intervals of slickwater stages are offset by intervals of crosslinked stages (McNeil et al, 2011). Analysis of field-wide core and well logs has resulted in a better understanding and the continued development of fracturing protocols in this formation. Today, treatments composed of intervals of increasing sand concentrations are common. The concentration of 30/50 mesh white sand is increased in a stepwise manner from 0.5 lb/gal up to a maximum of around 4 lb/gal, and 20/40 mesh sand is pumped at around 3 lb/gal at the tail end to maximize conductivity in the near wellbore region. Pumping schedules for two Eagle Ford wet gas/condensate wells near Kennedy, Texas that were completed in early 2014 appear in Appendix D and Appendix E.

Considering the high cost of a hydraulic fracturing treatment, the informed selection of treatment design parameters including proppant size and concentration, fracture fluid viscosity, and pumping profile is of great interest to operators in the Eagle Ford Shale. Therefore, understanding the behavior of fluids and proppants within a fracture and their relationship to fracture conductivity is invaluable.

1.2 Geology of the Eagle Ford Shale: zones and facies

The Eagle Ford Shale is an unconventional hydrocarbon reservoir that spans a length of 400 miles and a width of 50 miles across southwestern Texas. Named after the community of Eagle Ford outside of Dallas, one of several locations where shale outcrops occur above the surface, it has become one of the most active domestic plays since 2008 (Centurion et al., 2012). This reservoir encompasses three different hydrocarbon zones containing natural gas, liquid hydrocarbons, and crude oil (Fig. 1).

Classified as a carbonate-rich laminated reservoir, the Eagle Ford Shale was formed during the Late Cretaceous Period and deposited in a low-energy environment. Despite being labeled a shale, it is actually a mudstone composed of approximately 55% carbonate, 20% quartz, 15% clay, and 10% kerogen. However, mineral content varies widely across the reservoir; the samples used in this study are on average 72% carbonate, 20% quartz, 3% feldspar, and 2% clay. The reservoir is underlain by the Buda Limestone and overlain by the Austin Chalk (Viswanathan et al., 2011).

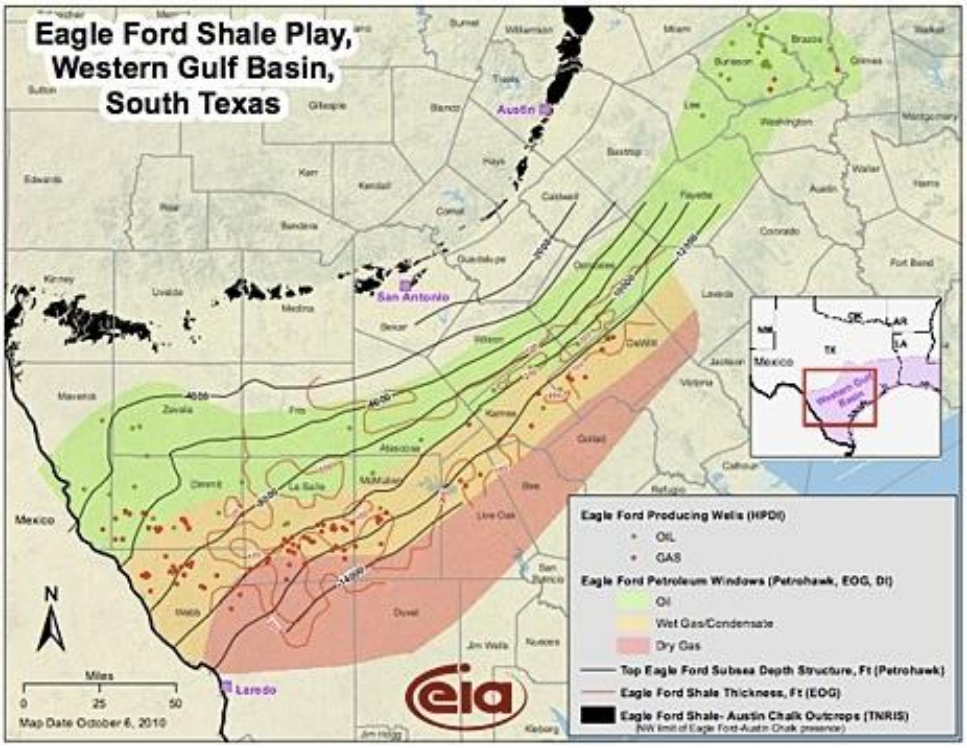

Fig. 1 –Three hydrocarbon zones: oil, condensate, and dry gas (US EIA, 2013)

It is subdivided into several vertical layers, or facies, based on the different lithological features of the strata (Gardner et al., 2013). In 2010, Donovan and Staerker divided the vertical layers into five facies, A – E, from the base up. A diagram identifying these facies appears in Fig. 2. Facies B has the highest total organic content levels in the formation and, therefore, is the common completion target of operators. It is unique from other shale reservoirs in that it is described as "self-sourcing"; the reservoir's hydrocarbons are thermogenically sourced from kerogen already present in the rock (Shelley et al., 2012)

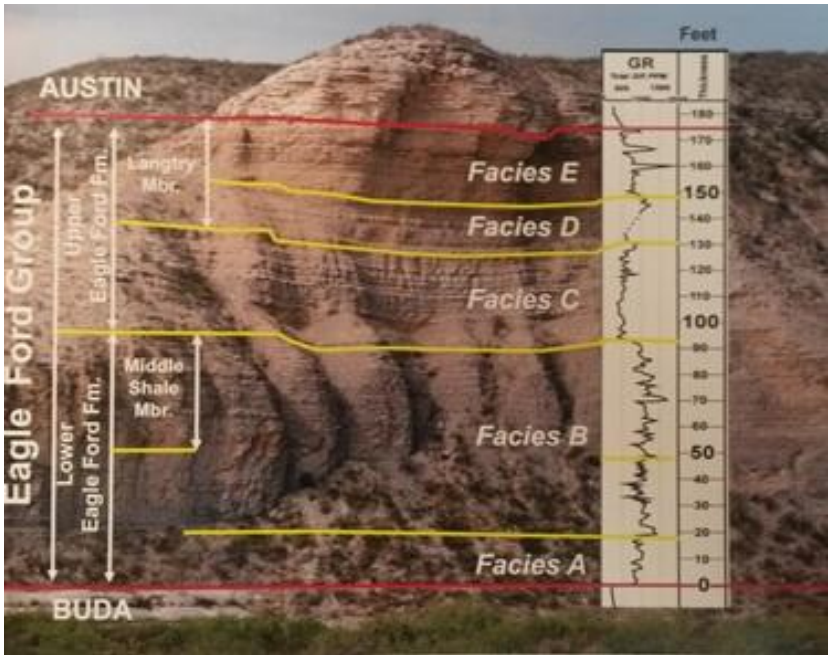

Fig. 2 – Schematic of facies A – E at the Lozier Canyon outcrop

Several reservoir characteristics vary significantly throughout the formation due to a difference in depositional environments. During the Late Cretaceous Period, the eastern region of the play was more elevated than the western region (Mullen et al, 2010). This elevation difference caused greater sediment deposition in the western basins and a variation in sediment composition across the formation. Traveling westward, the gross thickness increases from 20 to 500 feet thick and depth varies from 2,500 to 14,000 feet. Mineral composition varies in a comparable manner; quartz content ranges from 13% to 25% and is highest in the western regions, carbonate content ranges between 34% and 85% and is highest in the east (Quirein et al., 2013). Clay content fluctuates from 1% to 35%. TOC ranges from 2.1% to 5.2% of weight. Petrophysical properties differ as well; core porosities range from 1.5 to 9% and matrix

permeabilities from 0.001 to 0.0001 milliDarcies (Quirein et al., 2013). Recent geological analysis has identified that quartz, calcite, and clay content varies laterally even on the small scale of a single horizontal well (Gardner et al., 2013).

Studies of Eagle Ford Shale conclude that the effectiveness of a hydraulic fracturing treatment is influenced largely by the geological properties of the formation. Sahoo et al. (2013) identified that mineralogy, hydrocarbon filled porosity, and total organic content are most prominent parameters that control Eagle Ford well productivity. Mineral composition determines several geomechanical properties such as ductility, brittleness, and fracability that are tied to the effectiveness of a fracturing treatment. A field-wide analysis of Eagle Ford wells determined that wells with good production have a carbonate/quartz ratio greater than 4, clay volume less than 35%, and porosity greater than 5.5% (Sahoo et al., 2013). These studies show that an understanding of how geological properties affect a fracturing treatment is also a critical factor in successful reservoir development.

1.3 Literature review – partial monolayer theory and testing

Publications on the measurement of fracture conductivity in a laboratory setting date back to 1959, when Darin and Huitt flowed water through a proppant pack of steel balls placed between two steel plates and calculated the fracture permeability via a modified form of the Kozeny-Carman equation. Their results showed that a proppant pack of approximately one half of a monolayer achieved similar conductivity values to a multilayer proppant concentration of over 4.0 lb/ft^2. Their conclusions substantiated a

new theory; partial monolayer proppant packs could achieve higher conductivity values than a full monolayer or multilayer packs due to the "open porosity" between the grain spaces (Darin et al., 1959). Darin and Huitt's results appear in Fig. 3.

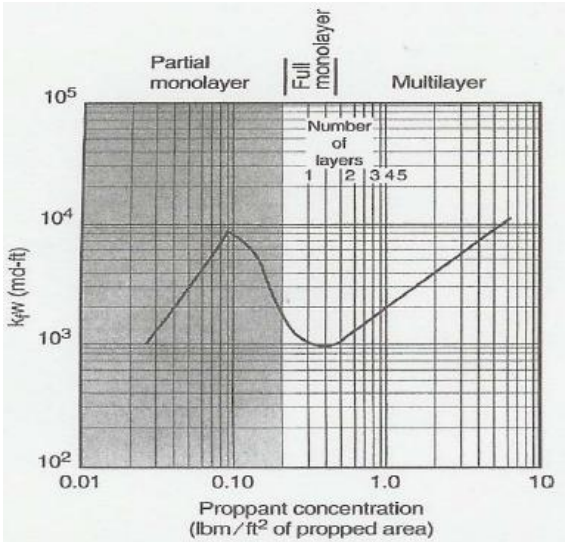

Fig. 3 – Fracture conductivity results of Darin and Huitt (1959)

The partial monolayer theory was dismissed by the industry for several decades because it was deemed "virtually impossible to achieve" in field fracturing treatments. Subsequent studies of the monolayer theory concluded that it was not possible to place a uniform partial monolayer in the reservoir due to the poor proppant transportability of available fracturing fluids (Brannon et al., 2004). Critics also cited the reduction of fracture width caused by proppant embedment and proppant crushing as additional factors that invalidated the partial monolayer theory (Wendorff et al., 1969) ; (Harrington et al.,1975).

In 1989, the partial monolayer theory was evaluated again by Gidley et al. (1989) and given theoretical support. Gidley indicated that a partial monolayer could theoretically achieve maximum conductivity, but field trials of the theory were not successful. Economides and Nolte (2000) reached similar conclusions; they stated that although a partial monolayer can create maximum fracture conductivity, placement of a partial monolayer in a vertical fracture in the reservoir is impossible to achieve.

In 1989, the American Petroleum Institute (API) released detailed testing guidelines titled API RP-61 in order to evaluate the conductivity of a proppant pack in a consistent laboratory setting. The procedure consists of placing 2 lb/ft^2 of proppant between metal shims and subsequently pumping a brine solution through the proppant pack. However, the API RP-61 procedure does not take the properties of a reservoir rock into account; as a result, conductivity measurements are significantly different when the metal shims are replaced with a lab sample with a rough fracture.

Laboratory measurement of fracture conductivity is also performed under far different conditions than in the field. Downhole factors including non-uniform proppant distribution within fractures, reduction of fracture width via proppant embedment, reduction of porosity by proppant crushing and migration, and non-Darcy flow effects can create significant differences between fracture conductivity measurements in the laboratory versus the field (Zhou et al., 2011). However, laboratory measurements are repeatable at standard conditions and therefore are used in several recent studies to evaluate the effects of different proppant concentrations on fracture conductivity.

Brannon et al. (2004) investigates the partial monolayer theory using a modified API RP-61 procedure. In this study, ½ inch flat Ohio Sandstone samples were propped with different concentrations of 20/40 mesh sand that ranged between partial monolayer and multilayer proppant packs. The results are the first published laboratory experiments that support the partial monolayer theory; Brannon's correlation between proppant concentration and fracture conductivity closely follows the trend described in Darin and Huitt (1959), and Brannon concludes that maximum fracture conductivity is obtained with a partial monolayer proppant pack.

More recent studies have also modified the API RP-61 procedure in order to study the short-term conductivity of other rock samples. Conductivity experiments using Berea sandstone sampless and very high concentrations of uncoated and resin coated ceramic proppant between 4 lb/ft^2, and 8 lb/ft^2 indicate that high closure stresses reduce fracture conductivity due to compaction of the proppant pack (Rivers et al., 2012). In multilayer proppant packs, uncoated proppant concentrations above 4 lb/ft^2 do not create higher fracture conductivity. Experiments using Barnett shale samples with rough fracture surfaces at low proppant concentrations between 0.03 lb/ft^2 and 0.2 lb/ft^2 determine that partial monolayer concentrations provide greater fracture conductivity than full monolayer concentrations at closure stresses below 3,000 psi (Kamenov et al., 2013). However, the conductivity of a partial monolayer decreases more rapidly with increasing closure stress due to proppant embedment and crushing. Therefore, the partial monolayer theory is not always valid at high closure stresses (Kamenov et al., 2013).

Current studies of the Eagle Ford Shale use field data to evaluate the effects of proppant concentration on production. However, there are no publications of Eagle Ford Shale that study the effects of proppant concentration on fracture conductivity in a laboratory setting. This study investigates the fracture conductivity of seven Eagle Ford Shale lab samples via unpropped and propped experiments using a modified API RP-61 procedure. Unpropped experiments were performed to obtain baseline conductivity measurements for comparison purposes. Propped experiments were performed at two proppant concentrations, 0.1 lb/ft^2 and 0.2 lb/ft^2 concentrations of 30/50 mesh white sand, to investigate the influence of proppant concentration on conductivity and the partial monolayer theory. The mineral composition of samples was also determined to identify any significant variations in content that could potentially alter conductivity measurements. Finally, surface profile scans were performed on one lab sample's rough fracture surface before and after conductivity tests to identify any permanent alterations in fracture surfaces caused by applied closure stresses.

1.4 Problem description

The variation in reservoir properties across the Eagle Ford formation is described in the literature as a "significant risk" to completion techniques that requires geophysical and geological analysis before application of hydraulic fracturing treatments. (Mullen et al, 2010). A recent publication determined that significant lateral variation can exist even on the small scale of a single horizontal well (Gardner et al., 2013). Studies also show that reservoir properties can affect the interaction between a rock and proppant and

therefore impact the fracture conductivity. As the cost of a fracturing treatment on a well in the Eagle Ford has drastically risen from $600,000 in 2009 to over $3.5 million today, there is an increasing need for the educated design and optimization of fracturing treatments in order to maximize hydrocarbon production and subsequent profits (Centurion, 2011).

This study examines the fracture conductivity of seven Eagle Ford Shale lab samples (labeled EF1 through EF7) that were collected from facies B. From the recovery standpoint, a critical parameter driving the design of a fracturing treatment is fracture conductivity. Therefore, fracture conductivity was chosen to be the performance indicator of fracturing treatment effectiveness in this study.

This study presents the results from a series of laboratory experiments performed on the seven lab samples. The experiments include propped and unpropped laboratory conductivity experiments, fracture surface profile scans, and mineralogical analysis of samples. By completing these objectives, this study is able to shed more light on the effect of different proppant concentrations on fracture conductivity in this unconventional reservoir.

1.5 Research objectives

The purpose of this study is to investigate the fracture conductivity of Eagle Ford Shale within the scale of a horizontal well and to evaluate the effect of proppant concentration on fracture conductivity. The seven samples of Eagle Ford Shale were collected from Comstock West (Fig. 4**)**, an outcrop site of facies B. This site is located

along Highway 90, approximately five miles west of the town of Comstock in Val Verde County, Texas.

Fig. 4 – Comstock West outcrop, the site of sample collection

EF1	EF2	EF3	EF4	EF5	EF6	EF7
	190 ft.	145 ft.	120 ft.	180 ft.	200 ft.	180 ft.

Table 1 – Distance between sampling locations

The samples were collected from the vertical face of the outcrop approximately 5 feet above the ground along the highway. Sampling locations were laterally spaced approximately 150 feet apart along a 1,015-foot lateral section of the outcrop. Table 1 shows the spacing between each sample collection site.

During conductivity experiments, 30/50 mesh white sand was the only proppant type used based on the literature and current pumping schedules in the Eagle Ford shown in Appendix D and Appendix E. Nitrogen gas was flown through the lab samples' fractures in order to simulate natural gas in a safe manner. This research encompasses the following objectives:

1. Implement a reproducible and consistent experimental procedure in order to measure the short-term fracture conductivity of Eagle Ford Shale lab samples. The laboratory procedures outlined in API RP-61 were generally followed; minor modifications are explained in detail in the following section.
2. Measure the propped and unpropped fracture conductivity of each lab sample. Propped experiments use only 30/50 mesh white sand and conductivity experiments are performed at two different proppant concentrations, 0.1 lb/ft^2 and 0.2 lb/ft^2.
3. Compare the results of unpropped and propped conductivity experiments. Also evaluate the variation in conductivity values between the seven samples within each experiment type: unpropped, 0.1 lb/ft^2 concentration, and 0.2 lb/ft^2 concentration.

4. Perform a fracture surface profile scan on a lab sample before and after an unpropped conductivity experiment in order to identify if permanent alterations to the sample's fracture surface are caused by high closure stresses.
5. Determine the mineral composition of each sample via FTIR in order to assess and compare content.

2. LABORATORY APPARATUS AND EXPERIMENTAL PROCEDURE

2.1 Description of laboratory apparatus

In order to standardize the experimental conductivity testing procedure in laboratories across the petroleum industry, the American Petroleum Institute released detailed testing guidelines titled API RP-61 in 1989. This document defines the required laboratory equipment and procedures for measuring fracture conductivity. This study follows the instructions in RP-61 with minor modifications, which are detailed below.

First, an API conductivity cell was used in this study to perform short-term conductivity experiments. Second, the metal plates specified by the document were replaced with lab samples with artificially induced fractures. The induced fractures have rough fracture surfaces and more accurately replicate actual fractures created in the reservoir during a fracturing treatment. Third, dry nitrogen gas was employed in this study as a working fluid instead of water or brine in order to simulate natural gas. Fourth, proppant concentrations of 0.1 lb/ft^2 and 0.2 lb/ft^2 were used instead of the standard 2 lb/ft^2 recommended by API RP-61.

Fracture conductivity was measured on the lab samples through a single crosscutting fracture that was manually induced in the rock. The samples were used to conduct two types of conductivity experiments, unpropped and propped. Unpropped experiments did not use proppant to widen the fracture aperture. For propped experiments, a specified concentration of 30/50 mesh white sand was inserted into the fracture prior to experiments. To prepare a sample for propped experiments, proppant was manually poured and spread evenly on the rough fracture surface. The sample was

subsequently loaded into a conductivity apparatus that allowed the user to apply a defined closure stress via a load frame and to flow nitrogen gas through the fracture. During the experiment, three datapoints were recorded: the gas flow rate, its pressure drop across the fracture, and the absolute cell pressure. These three variables were used to calculate fracture conductivity via Darcy's Equation.

The experimental apparatus consists of the following hardware:

- API conductivity cell
- CT-250 hydraulic load frame
- Nitrogen tank with mass flow controller
- Three pressure transducers
- Needle valve as a back pressure regulator
- Flow lines
- Data acquisition system

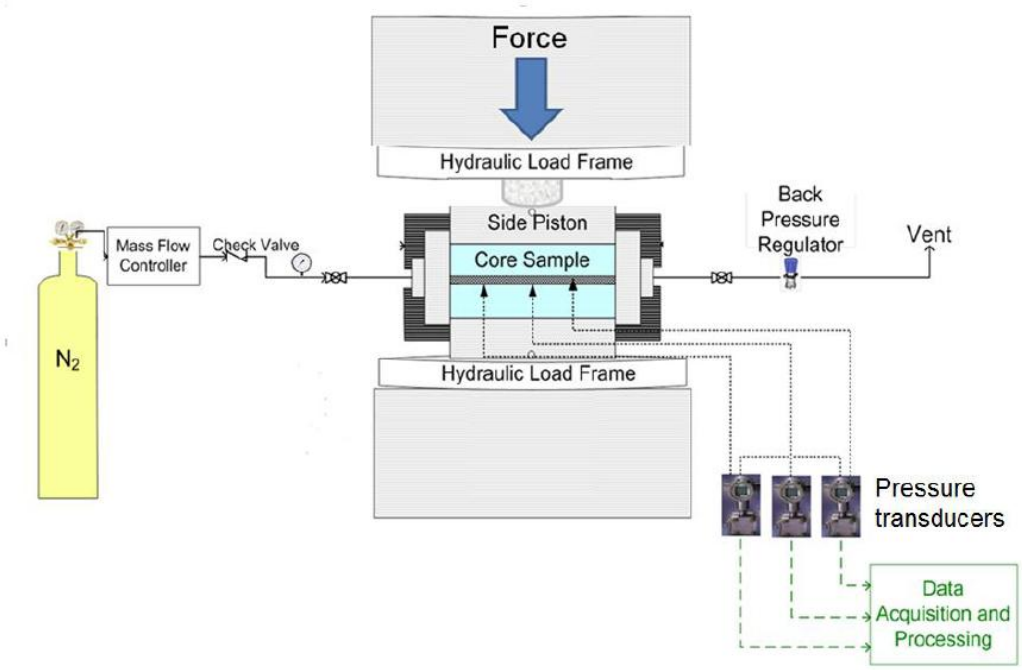

Fig. 5 – Diagram of testing apparatus, side view

Fig. 5 is a diagram of the testing apparatus. The API conductivity cell is placed under a hydraulic load frame that applies a specified closure stress to the lab sample. A nitrogen tank is connected to the conductivity cell and allows for the controlled flow of gas through the lab sample's fracture. Three pressure transducers are connected to the conducitivity cell along the fracture. The transducers measure absolute cell pressure and the pressure drop along the fracture length.

The API conductivity cell is constructed of 316 stainless steel and consists of five individual components that fit together: a cell body, an upper and lower piston, and a right and left flow insert. Fig 6 shows the components of the conductivity cell.

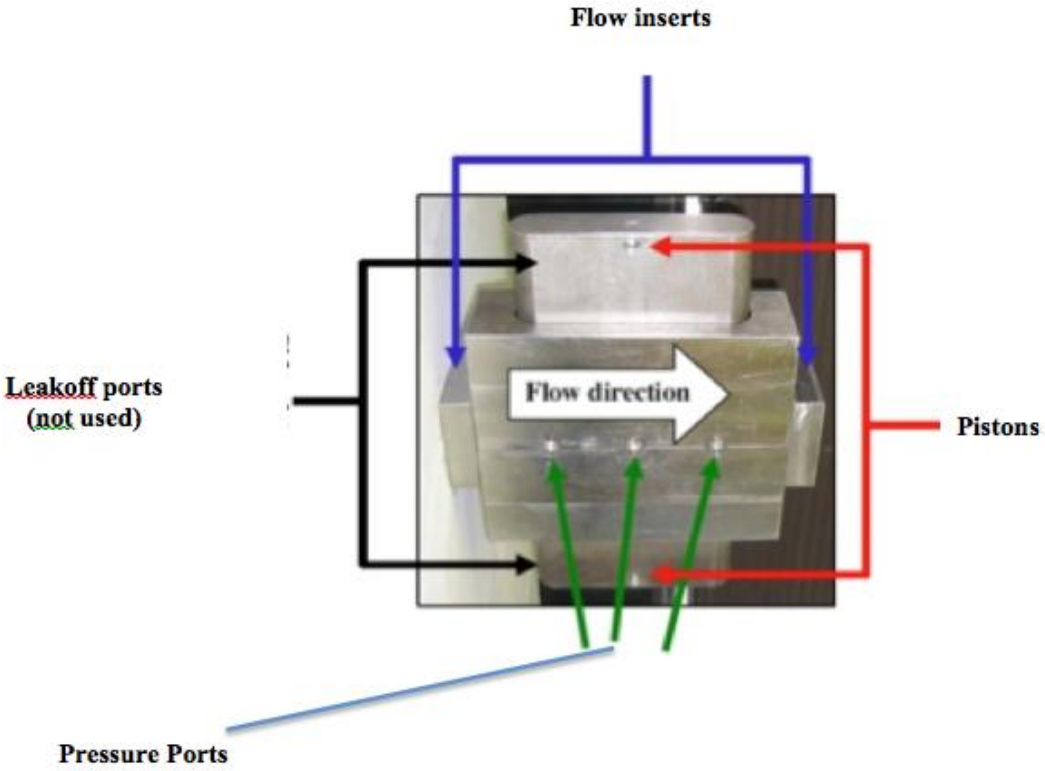

Fig. 6 – Modified API conductivity cell

The upper and lower pistons serve several purposes. They keep the lab samples at the correct depth within the cell body, allow the load frame to apply an evenly distributed vertical force to the sample, and prevent nitrogen gas leakage from the cell during experiments. The right flow insert serves as a gas intake port and connects the nitrogen tank's flow line to the cell body. The left flow insert is used to modulate the gas flow rate out of the cell; it has a needle valve that acts as a backpressure regulator, and that allows the user to precisely adjust the nitrogen gas flow rate through the fracture. Since fugitive gas leakage through fittings and connections causes inaccurate results, Viton polypack O-rings on each of the pistons and inserts create airtight

connections of these components to the cell body. The dimensions of the cell body (10 inches long, 3.25 inches wide, and 8 inches tall) allow a lab sample (7.25 inches long, 1.75 inches wide, and 6 inches tall) to press-fit tightly into its identically shaped cavity after preparation.

Three pressure-measuring ports on one of the cell body's vertical faces pass through the wall and are used during experiments to measure localized cell pressure within the fracture. The ports—left, right, and center—are located along a horizontal length of the cell body and match up with the sample's fracture when it is correctly positioned inside the cell body by the upper and lower pistons. The left and right transducers measure the pressure at both ends of the fracture, and the values are used to calculate the pressure drop across the length of the fracture. The center pressure transducer measures absolute pressure within the fracture. The three ports connect to a system of electronic pressure transducers that relay their pressure readings to the data acquisition system for output. The accuracy of the transducers is +/- 0.01 psi.

A nitrogen tank at 2,000 psi supplies a steady flow of gas to the conductivity cell. The flow of nitrogen from the tank is controlled by a spring valve that allows the user to precisely control the gas flow rate to the cell and through the fracture. During experiments, the conductivity cell is pressurized to approximately 55 psi and gas flow rates are kept below 2 liters per minute. An electronic mass flow controller on the tank's flow line measures the gas flow rate. The controller has a maximum measurement of 10 standard liters per minute and an accuracy of 0.001 standard liters per minute.

A hydraulic load frame is used to apply a specified closure stress to the cell via its actuating piston. It can apply a maximum force of 870 kN (195,584 lbf). Since the piston has a surface area of 10 in^2, this is equivalent to 19,00 psi maximum closure stress. The load frame is capable of changing its closure stress by 100 psi per minute. The axial displacement of its piston is measured at an accuracy of 0.01 millimeters.

2.2 Lab sample preparation

The five main steps necessary to prepare a piece of shale collected from the outcrop for an experiment are outlined below (Fig. 7).

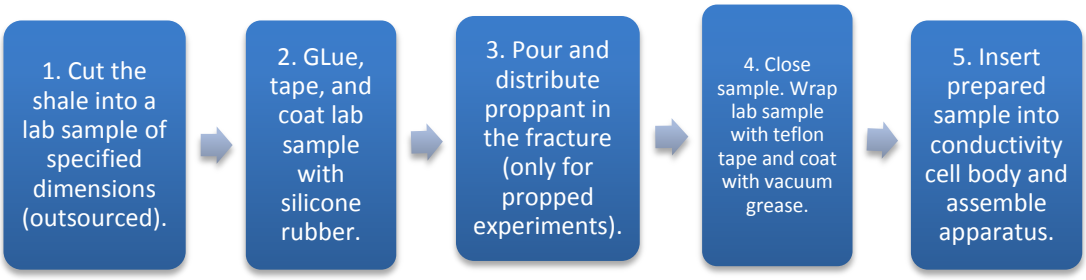

Fig. 7 – Steps of lab sample preparation.

2.2.1 Lab sample preparation for an unpropped experiment

The Eagle Ford Shale samples collected from the outcrop site were cut into lab samples of specified dimensions (7 inches long, 1.65 inches wide, and 2 inches tall) that match the geometry of the cell body's cavity. Due to the brittle nature of the shale, lab samples have a tendency to break apart during masonry preparation and experimental testing. Therefore, the two sections of a lab sample (upper and lower) were sandwiched

between and glued to identically shaped, 2-inch tall Berea sandstone samples (Fig. 8). Sandstone, with its softness and durability, creates a sturdy foundation for the brittle shale sections.

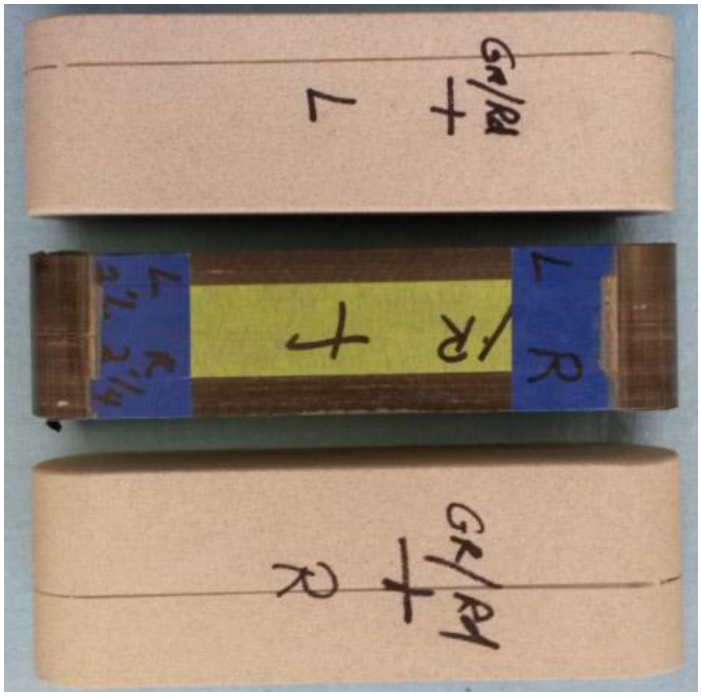

Fig. 8 – Unprepared lab sample configuration

At Kocurek Industries, a local masonry shop, a single crosscutting fracture was carefully induced in each of the lab samples along the laminated bedding plane. This created a rough fracture surface that is similar to fractures created in the reservoir during a field-scale hydraulic fracturing treatment. The loose sediment and infill material commonly found in the fractures of prepared samples from other shale types are typically left in place for experimental testing. However, loose material was not found in any of these fractures.

Prior to coating the lab sample with silicone sealant, a single layer of masking tape was banded around the shale's crosscutting fracture in order to prevent leakage of the liquid sealant into the fracture during the rubber epoxy coating procedure. In addition, three layers of primer were applied to the sample in order to increase the bond strength of the sealant to the lab sample's outer surface. The next step in lab sample preparation was the coating of the sample with a thin layer of silicone rubber. This outer layer creates a tight seal between the prepared lab sample and the conductivity cell, preventing leakage of nitrogen gas during experiments. The coating procedure is performed by placing the lab sample into a preparation mold (Fig. 9), which has a cavity that matches the geometry of the conductivity cell's cavity. Liquid silicone rubber is then poured into the void between the lab sample and the mold, and the mold is baked in an oven at 150^{O}F to solidify it.

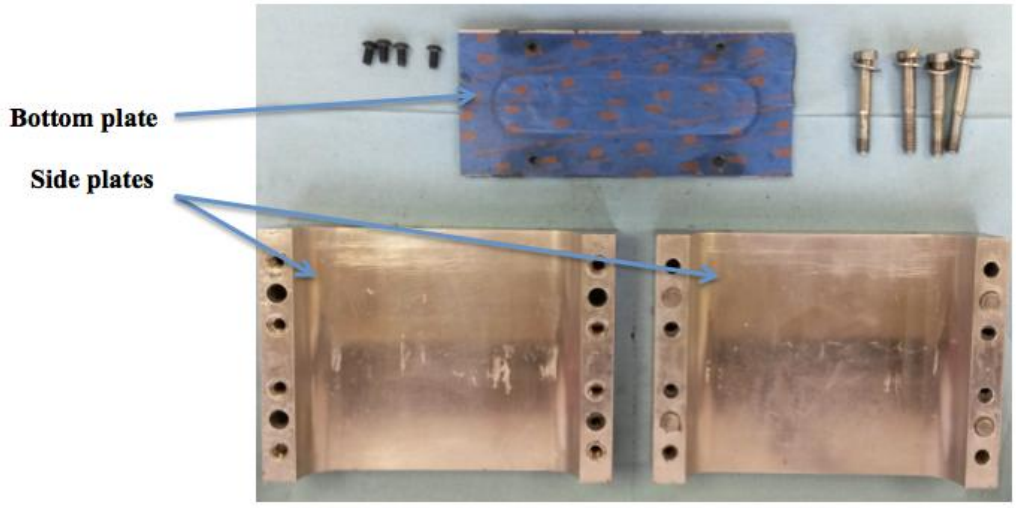

Fig. 9 – Components of preparation mold

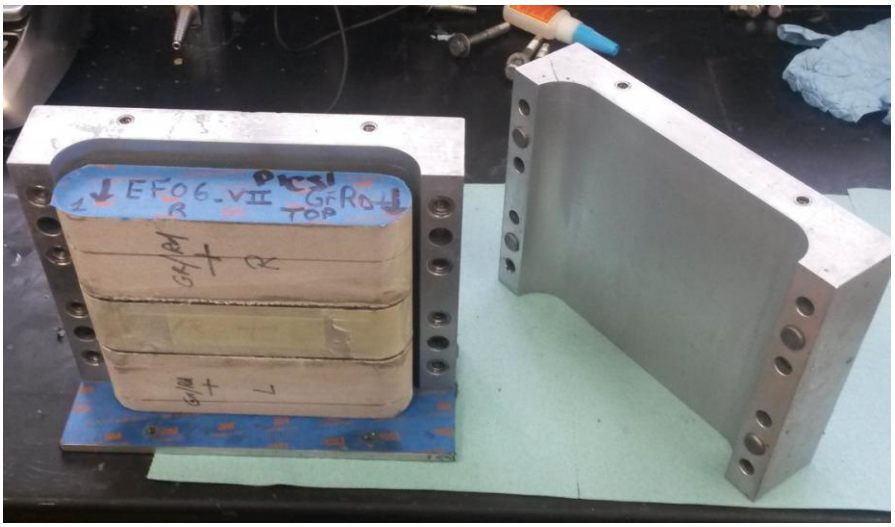

Fig. 10 – Sample in preparation mold (step 9)

Fig. 9 and Fig. 10 illustrate the components used in the procedure. Using a 6-inch tall preparation mold, the coating of the lab samples was completed in a single stage. The detailed preparation procedure for a single stage preparation is outlined below:

1. Glue the fractured lab sample between the two sandstone samples using Gorilla Glue. Place a heavy weight on top of it and allow it to dry for 24 hours.
2. Using a razor blade, remove any excess dried glue extruding from the interfaces.
3. Wrap a single band of masking tape around the circumference of the lab sample's fracture.
4. Apply painter's tape to the top and bottom faces of the sandstone samples to ease in post-preparation clean up. Cut the tape to the surfaces' dimensions and write the sample's number on the painter's tape for identification.
5. Apply silicone primer to the outer surface of the lab sample with a brush. Apply the primer three times and wait 10-15 minutes between each application.

6. Thoroughly clean the inner surface of the preparation mold with acetone and paper towels.
7. Spray silicone release agent onto the inner faces of the preparation mold. Spray inner faces three times and wait 3-5 minutes between each application.
8. Weigh out 120 grams of silicone potting compound and 120 grams of silicone curing agent from the RTV 627 022 kit in a single Styrofoam cup. Make sure that the mixing ratio is 1:1 using a gram scale. Avoid contamination with small particles or debris. Mix and stir the fluids together with a stirring device such as a pencil. Allow the mixture to settle for 20 minutes in order to release any air bubbles trapped in the suspension while mixing.
9. While the silicone mixture is settling, assemble the 6-inch preparation mold: Tightly screw the bottom plate onto either one of the mold's side plates. Carefully place the lab sample in the center of the mold, leaving an even space between the sample and the mold around the entire circumference (Fig. 10). Match up the mold's second side plate and tightly screw the mold's side plates together. Screw in the bottom plate to the second side plate. Ensure that the sample does not contact the sides of the mold's plates.
10. Pour the silicone mixture slowly into one side of the mold until the space between the sample and the mold is filled. A tool such as a spackling knife can aid in pouring. It is essential to pour the silicone mixture from one side of the mold to prevent air bubbles from being trapped in the mixture; bubbles will result in a poorly coated sample and may result in leakage during experiments. After

the lab sample is fully submerged in the liquid silicone mixture, tap the mold with a wrench to facilitate the release of any air bubbles suspended in the fluid.

11. Let the mold sit for one hour, checking for any leakage of silicone mixture. Tighten screws and bolts if necessary.
12. Place the mold in the laboratory oven and cook it for three hours at 150°F.
13. Remove the preparation mold from the oven and let it cool for one hour.
14. Loosen the screws and bolts on the preparation mold. Using a hydraulic jack, manually push the lab sample out of the mold.
15. Cut the solid silicone edges along the sample's top and bottom with a razor blade in order to round the edges. This will make insertion of the prepared lab sample into the cell body easier.
16. Cut three square windows in the silicone sealant that match up with the locations of the conductivity cell's pressure ports. Cut two circular windows on the ends of the sample to match up with the flow inserts. These holes serve as an inlet and outlet for the nitrogen gas. A prepared sample in this manner appears in Fig. 11.

Fig. 11 – Coated sample with three windows cut

17. Wrap a horizontal band consisting of 2 layers of silicone plumbing tape around the base of the sample. Wrap an identical horizontal band directly above the windows that were cut in step 16. Wrap two vertical band consisting of two layers of the tape between each of the three square windows. See Fig. 12 at the end of section 2.2.2 for placement of silicone tape bands.
18. Coat the sample in vacuum grease, starting along the silicone tape bands, in order to hold them in place. The grease eases the insertion of the lab sample into the conductivity cell. In addition, it creates an airtight seal between the conductivity cell and the silicone layer on the lab sample, preventing nitrogen gas leakage from the cell. The lab sample is now prepared and ready to be inserted into the cell body of the testing apparatus for an unpropped experiment. Proceed with assembly of laboratory apparatus in section 2.3.

2.2.2 Lab sample preparation for a propped experiment

To prepare a lab sample for a propped experiment, the proppant is manually poured and evenly distributed on the fracture surface. Two types of propped experiments were performed using different proppant concentrations, 0.1 lb/ft^2 and at 0.2 lb/ft^2. 3.2 grams of proppant evenly distributed on the fracture surface is equal to a concentration of 0.1 lb/ft^2 and 6.4 grams is equal to 0.2 lb/ft^2 concentration.
The detailed procedure for placement of proppant within the fracture is explained below.

1. After completion of the unpropped experiment, turn off the data acquisition system and disassemble the testing apparatus as described in steps 17 through 25 of Section 2.4 below. Manually push the lab sample out the cell body with the hydraulic press.
2. Wipe the vacuum grease from the outer surfaces of the sample and remove the bands of silicone tape. Lay the sample down on a flat surface and use a razor blade to cut through the rubber sealant around the circumference of the fracture. The fracture typically acts as a guide for the razor blade during cutting. Carefully separate the top and bottom lab sample pieces. The fracture surfaces of a separated lab sample appear in Fig. 12.
3. After separating the two pieces of the lab sample, place the bottom piece of the lab sample on a sheet of paper.
4. Weigh the desired amount of proppant in a cup on a gram scale, 3.2 or 6.4 grams.
5. Pour and evenly distribute the proppant onto the fracture surface of the sample's bottom piece with your finger. Carefully position and align the sample's top

piece on top of the bottom sample piece, making sure all proppant remains in the fracture. Collect any loose proppant from the sheet of paper and place onto the fracture. Repeat steps 17 and 18 in section 2.2.1 above to coat and wrap the sample with Teflon tape. A cut lab sample with proppant inserted in the fracture and bands of Teflon tape appears in Fig. 13. The lab sample is now prepared and ready to be inserted into the cell body of the testing apparatus for a propped experiment. Proceed with assembly of laboratory apparatus in section 2.3.

Fig. 12 – Fracture surfaces of a lab sample after being cut open

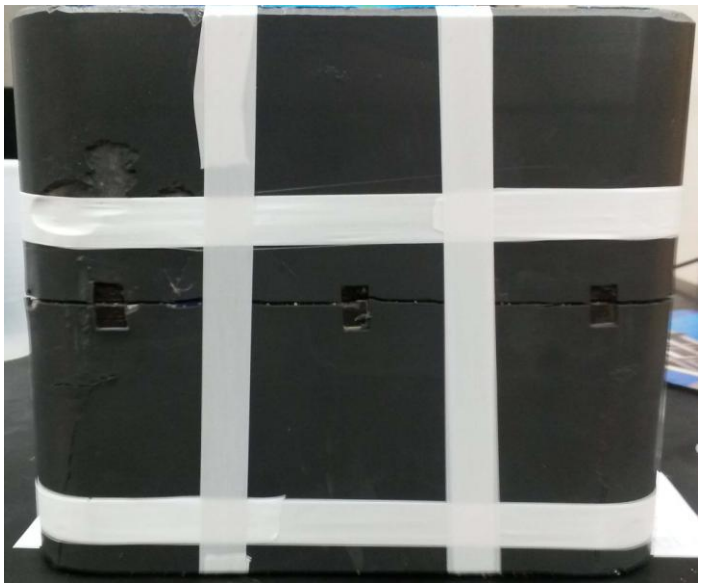

Fig. 13 – A lab sample with Teflon tape bands applied

2.3 Assembly of laboratory apparatus

1. Manually insert the prepared lab sample into the cell body of the conductivity apparatus using a hydraulic press so that the top of the sample is approximately 1 inch from the top of the cell.
2. Carefully lift the loaded cell body and place it on top of the bottom piston. Avoid tilting or shaking the cell to avoid rearranging the proppant. To prevent gas leakage, coat the rubber O-rings on the bottom and top pistons with high-temperature o-ring lubricant before insertion.
3. Insert the screw plug into the leak-off port in the bottom piston. Wrap Teflon tape around the threaded section of the plugs to create an airtight seal.
4. Insert the top piston into the top of the conductivity cell and place the assembled

conductivity cell under the load frame's piston. Apply a 1,000 psi closure stress to the cell.

5. Insert the screw plug into the leak-off port of the top piston with Teflon tape.
6. Mount and screw in the left and right flow inserts.
7. Connect the flow line from the nitrogen tank to the right insert. Connect the pressure transducers to the three pressure ports.
8. The setup is ready for conductivity measurements. Proceed with conductivity experiment as described in section 2.4. Fig. 14 shows a picture of the fully assembled conductivity setup under the load frame**.**

Fig. 14 – Assembled laboratory apparatus

2.4 Fracture conductivity experiment

In this study, short-term fracture conductivity experiments were performed using dry nitrogen gas to simulate natural gas production through fractures in Eagle Ford Shale. Experiments were performed at room temperature. Six separate trials were performed during each conductivity experiment at six static closure stresses, 1,000 through 6,000 psi at 1,000 psi increments. During each trial, measurement of two variables, absolute cell pressure and pressure drop, was recorded at four different gas flow rates. Nitrogen gas flow rates, ranging between 0.25 liters per minute (lpm) and 2 lpm, were also recorded. These three values were then used to calculate conductivity using a modified form of Forchheimer's equation.

The step-by-step procedure to measure fracture conductivity is explained below:

1. Complete the procedure explained in section 2.2.1 for unpropped experiments or section 2.2.2 for propped experiments. Insert the sample into the conductivity cell and assemble the testing apparatus as described in section 2.3.
2. Turn on and set-up the data acquisition system on the computer. Plug in the mass flow controller.
3. Fully close the backpressure regulator attached to the left flow insert.
4. Fully open the valve on the nitrogen tank.
5. Once a closure stress of 1,000 psi by the load frame, carefully turn the spring valve on the nitrogen tank clockwise. Nitrogen gas will begin flowing into the cell. Continue to open the tank valve until the cell pressure reaches approximately 55 psi. Wait until the reading stabilizes. To avoid disturbing

proppant placement during propped experiments, slowly pressurize the cell at flow rates less than 2 liters per minute

6. Check for cell leakage. The baseline gas flow rate should not be above 0.35 liters per minute. Higher flow rates indicate fugitive gas leakage in the system and will result in inaccurate conductivity results. If baseline values are above 0.35 lpm, it is probable that the sample will need to be extracted and re-prepared.
7. Record the baseline output values of flow rate, cell pressure, and pressure drop while the back pressure regulator is closed. The baseline values of flow rate and pressure drop are subtracted from the measured values in order to zero them.
8. Slowly open the back pressure regulator on the left flow insert by twisting it counterclockwise. Increase the flow rate until pressure drop increases by approximately 0.1 psi. Wait until the readings of flow rate, cell pressure, and pressure drop stabilize. Maintain a constant cell pressure between 50-55 psi during all measurements.
9. Record the flow rate, cell pressure, and pressure drop values.
10. Increase the flow rate by adjusting the backpressure valve. Wait until the output values stabilize. Record the values of the three outputs above. For measurement accuracy, the pressure drop value must not exceed 10% of the cell pressure. (This is due to gas's high compressibility.)
11. Repeat steps 6 through 10 two more times for a total of four measurements at each closure stress. This ensures the consistency and accuracy of the measurement from a statistical standpoint. Do not exceed a flow rate of 2.0 liters

per minute in order to avoid turbulent flow and non-Darcy flow effects.

12. Fully close the back pressure regulator.
13. On the computer, increase the load frame's closure stress to 2000 psi. During 5000 and 6000 psi trials, leave the back pressure regulator slightly open to prevent any excessive gas pressure build up in the fracture during the process.
14. Once closure stress has been increased to 2000 psi, allow the system to stabilize for 15 minutes.
15. Record the three baseline measurements, as described in step 7. Repeat steps 8 through 11 and record measurements at four different gas flow rates.
16. Proceed to perform trials between 3000 and 6000 psi in the same manner. Use similar flow rates for the data points at each closure stress.
17. After recording data points at 6000 psi, stop the flow of nitrogen gas via the spring valve on the tank.
18. Slowly bleed the pressure from the system by opening the backpressure regulator and the purge valve on the gas flow line. Decrease the cell pressure to baseline. Ensure that different pressure does not exceed the maximum pressure rating of the diaphragms in the pressure transducers.
19. Unscrew the gas flow line and the pressure transducers. Unscrew and remove the flow inserts and the piston plugs. This is done easily while a closure stress is applied.
20. Use the Labview program to lift the load frame's piston so it is no longer in contact with the top piston of the cell body.

21. Remove the top piston and bottom piston from the cell body.
22. Press the lab sample out of the disassembled cell body using the hydraulic frame.
23. Turn off the load frame hydraulic pump and the data acquisition system.
24. Bleed off the pressurize gas between the tank and its spring valve: Make sure the flow line is disconnected. Slowly open the spring valve until the hardware is de-pressurized.
25. Unplug the flow rate monitoring device.
26. Clean the cell using a degreasing agent and paper towels.

2.5 Darcy's law for an incompressible fluid

Darcy's law is an equation that describes the movement of a viscous incompressible fluid through a porous medium. Darcy's law for one-dimensional horizontal flow appears below in equation (2-1) and a diagram of the variables appears in Fig. 15.

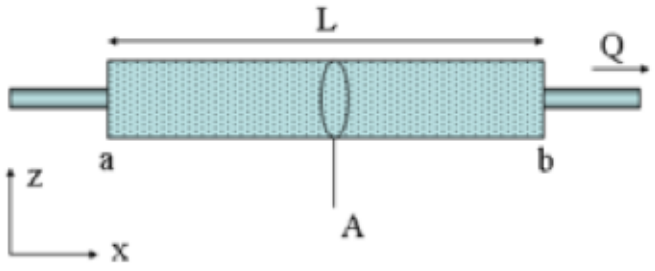

Fig. 15 – Diagram of Darcy's law variables

$$Q = \frac{kA}{\mu}\frac{p_a - p_b}{L} \qquad \textbf{(2-1)}$$

In equation (2-1), Q is the fluid's volumetric discharge rate from the medium, k is the permeability of the porous medium, A is the cross-sectional area normal to flow, $(p_a - p_b)$ is the pressure drop, L is the length over which the pressure drop takes place, and μ is the fluid's dynamic viscosity.

The Darcy unit is defined such that a porous medium with a cross sectional area of 1 cm^2 and a permeability of 1 Darcy will transmit 1 cc of water with a viscosity of 1 centipoise per second, providing that the pressure drop is 1 atm/cm. Darcy's Law is applicable only in the case of laminar flow, assuming fluid properties are constant.

Darcy flux v (cm/s) is calculated by dividing the volumetric discharge rate Q by the cross-sectional area A normal to flow.

$$v = \frac{Q}{A} \qquad \textbf{(2-2)}$$

Darcy flux is not the velocity at which the fluid flows through the pores in the medium; since the fluid needs to squeeze through the pore space, the fluid travels at a faster rate through the porous medium.

In equation (2-1), $\frac{p_a - p_b}{L}$ can be expressed as a derivative $\frac{dp}{dl}$, the pressure drop gradient in the direction of flow. Replacing this term and including the Darcy flux, equation (2-1) becomes:

$$\frac{dp}{dL} = \frac{\mu v}{k} \qquad \textbf{(2-3)}$$

2.6 Fracture conductivity calculation for a compressible fluid

Equation (2-3) can be combined with the real gas law and the gas flux equation in order to calculate fracture conductivity for a compressible fluid. Fracture conductivity is calculated with the three variables recorded during conductivity experiments: cell pressure p_{cell} (psi), differential pressure Δp (psi), and gas flow rate q (L/min). The three equations are given below:

Darcy's law

$$\frac{dp}{dL} = \frac{\mu v}{k} \tag{2-4}$$

Real gas law

$$\rho = \frac{pM}{zRT} \tag{2-5}$$

Gas flux

$$\frac{W}{A} = \rho v \tag{2-6}$$

The variables in the real gas law are density ρ (kg/m^3), pressure p (Pa), relative molecular mass of nitrogen M (kg/mol), gas compressibility factor z, the universal gas constant R (J/mol K), and temperature T (K).

The variables in the gas flux equation are mass flow rate W (kg/sec), cross sectional area normal to flow A (m^2), gas density ρ (kg/m^3), and gas velocity v (m/sec). Table 2 at the end of this section shows the values and units of the variables.

Equation (2-4) is multiplied by the gas density ρ and the equation is rearranged to get *dp* and *dL* on opposite sides of the equation:

$$\rho(dp) = \frac{\mu v}{k}\rho(dL) \quad \textbf{(2-7)}$$

The gas flux equation (2-6) is then rearranged in order to solve for gas density ρ:

$$\rho = \frac{W}{Av} \quad \textbf{(2-8)}$$

Substituting equations (2-5) and (2-8) into equation (2-7) yields:

$$\frac{pM}{zRT}\,dp = \frac{\mu v}{k}\frac{W}{Av}\,dL \quad \textbf{(2-9)}$$

Equation (2-9) simplifies to:

$$\frac{pM}{zRT}\,dp = \frac{\mu}{k}\frac{W}{A}\,dL \quad \textbf{(2-10)}$$

The derivatives in equation (2-10) are put in integral form:

$$\frac{M}{zRT}\int_2^1 p\,dp = \frac{\mu}{k}\frac{W}{A}\int dL \quad \textbf{(2-11)}$$

Integrating the *dp* and *dL* in equation (2-11) yields:

$$\frac{M}{zRT}\frac{(p_1^2 - p_2^2)}{2} = \frac{\mu}{k}\frac{W}{A}L \quad \textbf{(2-12)}$$

The gas velocity *v* in the fracture is equal to $\frac{q}{w_f h_f}$, where w_f is the fracture aperture and h_f is the height of the fracture face. Therefore the gas flux equation in equation (2-8) can be written as:

$$\frac{W}{A} = \frac{q\rho}{w_f h_f} \quad \textbf{(2-13)}$$

Plugging equation (2-13) into equation (2-12) yields:

$$\frac{M(p_1^2-p_2^2)}{2zRTL} = \frac{\mu q \rho}{h_f}\frac{1}{w_f k_f} \quad \textbf{(2-14)}$$

In the expression $\frac{M(p_1^2-p_2^2)}{2zRTL}$ plotted on the y-axis, $(p_1^2 - p_2^2)$ is calculated from the p_{cell} and Δp measurements. p_{cell} is measured by the middle of the three pressure transducers along the fracture and is the average cell pressure along the length of fracture that is measured by the three transducers; although the length of the entire fracture surface is 7.25 inches, the three transducers measure only the pressure along 5.25 inches of the fracture. The Δp is the difference between the right transducer (higher pressure) at the inlet and left (lower pressure) transducer at the outlet, $\Delta p = p_1 - p_2$. For the y-axis calculation, $(p_1^2 - p_2^2)$ is calculated as follows. p_{cell} is the average of pressure readings of the right and left transducers.

$$p_{cell} = \frac{p_1+p_2}{2} \quad \textbf{(2-15)}$$

Rearranging equation (2-15):

$$2\, p_{cell} = p_1 + p_2 \quad \textbf{(2-16)}$$

Therefore multiplying 2 times the P_{cell} by the Δp yields:

$$2\,(p_{cell})(\Delta p) = (p_1 + p_2)(p_1 - p_2) = (p_1^2 - \, p_2^2) \quad \textbf{(2-17)}$$

14.7 psi is added to each of the pressures in order to convert gage pressure (psig) to absolute pressure (psia). $(p_1^2 - p_2^2)$ is then converted from units of psia^2 to Pascals^2 $(\frac{1\ \text{kg}}{\text{m s}^2})^2$ by multiplying by $\left(\frac{6894.8\text{Pa}}{1\ \text{psia}}\right)^2$.

In the y-axis equation $\frac{M(p_1^2-p_2^2)}{2zRTL}$, T is the gas temperature at a room temperature of 68^{O}F, or 293.15 K. The temperature conversion appears below:

$$K = \frac{F-32}{1.8} + 273.15 \quad \textbf{(2-18)}$$

The length of the fracture over the pressure drop, L = 5.25 inches, is converted to meters.

$$L = 5.25 \text{ in } \left(\frac{1 \text{ m}}{39.37 \text{ in}}\right) = 0.1335 \text{ m} \quad \textbf{(2-19)}$$

The expression $\frac{M(p_1^2-p_2^2)}{2zRTL}$ on the y-axis therefore has units of $\frac{1}{\text{m}^3}$.

In the expression $\frac{\mu q \rho}{h_f}$ on the x-axis, the viscosity μ and the density ρ of the nitrogen gas are at room temperature. The nitrogen gas flow rate q, measured in liters/minute, is converted to m^3/second by the conversion below.

$$q = \left(\frac{\text{Liters}}{\text{minute}}\right)\left(\frac{1 \text{ m}^3}{1{,}000 \text{ L}}\right)\left(\frac{1 \text{ minute}}{60 \text{ seconds}}\right) \quad \textbf{(2-20)}$$

The height h_f of the fracture face is converted to meters.

$$h_f = 1.65 \text{ in } \left(\frac{1 \text{ m}}{39.37 \text{ in}}\right) = 0.0419 \text{ m} \quad \textbf{(2-21)}$$

At a given closure stress, four sets of X-axis and Y-axis values are calculated for each dataset (gas flow rate *q*, cell pressure p_{cell}, and pressure drop (Δp). The four data points are then plotted on a graph and a linear trend line is applied to the data points. Fig. 16 is a graph of data collected during a propped experiment (0.1 lb/ft^2) at 6,000 psi closure stress.

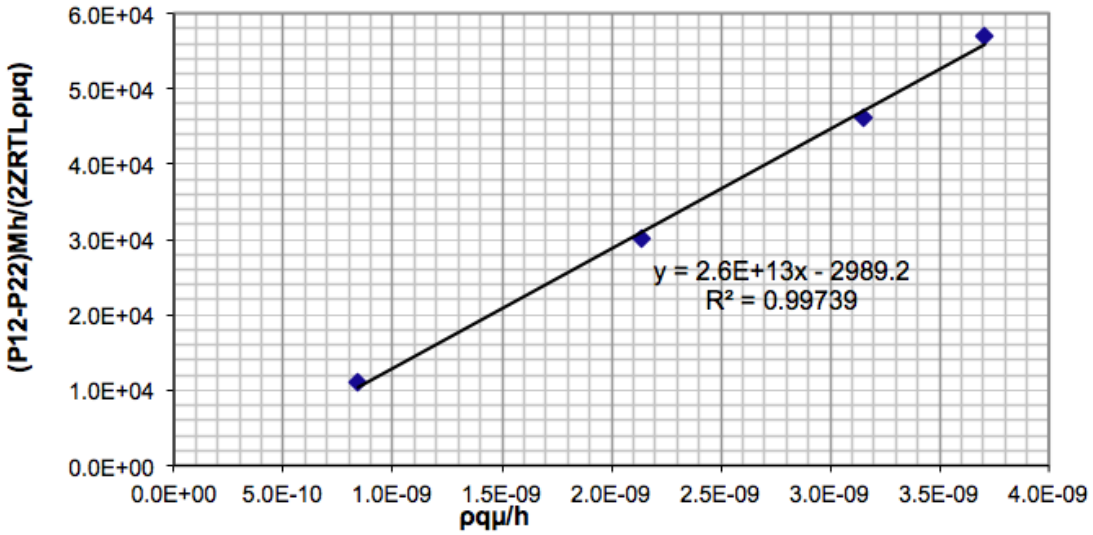

Fig. 16 – Graph for calculating conductivity

The slope of the line is equal to the inverse of fracture conductivity $k_f w_f$, where k_f is fracture permeability and w_f is fracture width. Equation (2-22) is used to calculate fracture conductivity in units of milliDarcy-feet.

$$k_f w_f = \left(\frac{1}{\text{slope}}\right)\left(\frac{1}{9.869\text{x } 10^{-16}\text{ m}}\right)\left(\frac{1\text{ m}}{0.0254\text{ in}}\right)\left(\frac{1\text{ ft}}{12\text{ in}}\right) \quad \textbf{(2-22)}$$

$$k_f w_f = \left(\frac{1}{2.6\text{ x } 10^{13}}\right)\left(\frac{1}{9.869\text{x } 10^{-16}\text{ m}}\right)\left(\frac{1\text{ m}}{0.0254\text{ in}}\right)\left(\frac{1\text{ ft}}{12\text{ in}}\right) \quad \textbf{(2-23)}$$

$$k_f w_f = 127.9\text{ mD} - \text{ft} \quad \textbf{(2-24)}$$

	Variable	Value	Unit
Cell Pressure	P_{cell}	measured	psi
Differential Pressure	Δp	measured	psi
Compressibility factor	z	1	
Universal gas constant	R	8.3144	J/mol-K
Temperature	T	293.15	K
RMM of nitrogen	M	0.028	kg/mol
Viscosity of nitrogen	μ	1.76E-05	Pa s
Density of nitrogen	ρ	1.16085	kg/m^3
Width of fracture	h_f	1.65	in.
Length over pressure drop	L_f	5.25	in.

Table 2 – Variables and units in conductivity calculation

2.7 Proppant unit conversion calculations

To relate the two amounts of proppant used in the conductivity experiments to proppant concentrations in lb/gal that are used during field-scale hydraulic fracturing treatments, a series of calculations are performed. First the areal proppant concentration on the fracture surface is calculated. 3.2 grams of proppant was placed on a fracture surface of with an area of 10 in^2.

$$3.2\text{g}\left(\frac{1\text{ lb}}{453.592\text{ g}}\right) = 0.0071\text{ lb} \quad \textbf{(2-25)}$$

$$10\text{ in}^2\left(\frac{1\text{ ft}}{12\text{ in}}\right)^2 = 0.0694\text{ ft}^2 \quad \textbf{(2-26)}$$

Therefore the areal proppant concentration on the fracture surface is:

$$\frac{0.0071\text{ lb}}{0.0694\text{ ft}^2} = 0.102\frac{\text{lb}}{\text{ft}^2} \quad \textbf{(2-27)}$$

The areal proppant concentration is converted to the volumetric concentration within the fracture by dividing it by the dynamic fracture width $w_{dynamic}$ of 0.2 inches. $w_{dynamic}$ is divided by 12 to convert inches to feet.

$$0.102 \ \frac{\text{lb}}{\text{ft}^2}\left(\frac{1}{0.2 \text{ in}}\right)\left(\frac{12 \text{ in}}{1 \text{ ft}}\right) = 6.12 \frac{\text{lb}}{\text{ft}^3} \quad \textbf{(2-28)}$$

Cubic feet are converted to gallons.

$$6.12 \frac{\text{lb}}{\text{ft}^3}\left(\frac{1 \text{ ft}^3}{7.48052 \text{ gal}}\right) = 0.82 \frac{\text{lb}}{\text{gal}} \quad \textbf{(2-29)}$$

Therefore

$$3.2 \text{ grams} = 0.1 \frac{\text{lb}}{\text{ft}^2} = 0.82 \frac{\text{lb}}{\text{gal}} \quad \textbf{(2-30)}$$

6.4 grams of proppant has twice the concentration:

$$6.4 \text{ grams} = 0.2 \frac{\text{lb}}{\text{ft}^2} = 1.64 \frac{\text{lb}}{\text{gal}} \quad \textbf{(2-31)}$$

The propped conductivity experiments that used 3.2 grams of sand are comparable to pumping 0.82 lb/gal of proppant in the field during a fracturing treatment. The conductivity experiments that used 6.4 grams of proppant are comparable to twice that concentration, or 1.64 lb/gal. Both 0.82 lb/gal and 1.64 lb/gal are within the range of concentrations pumped in the initial stages of a step-wise fracturing treatment (Appendix D) (Appendix E).

2.8 Propped fracture width and proppant layer calculations

To determine the propped fracture widths and number of proppant layers at 0.1

lb/ft^2 and 0.2 lb/ft^2 concentrations, a series of calculations are performed. The properties of Northern White Sands 30/50 mesh proppant supplied by CRS Proppants are used in the calculations below. At 0.1 lb/ft^2 concentration, 3.2 grams of sand with a density of 2.65 g/cm^3 are evenly distributed across the fracture surface. ISO 13502-2, a document that standardizes proppant sieve sizes, states that the diameter of 30/50 mesh proppant is between 0.03 cm and 0.06 cm. Therefore the average proppant diameter is 0.045 cm. The volume of 3.2 grams of proppant is calculated by dividing the proppant mass by the proppant density.

$$V_{prop} = \frac{m_{prop}}{\rho_{prop}} \quad \textbf{(2-32)}$$

$$V_{prop} = 3.2\ \text{g} \left(\frac{1\ \text{cm}^3}{2.65\ \text{g}}\right) = 1.208\ \text{cm}^3 \quad \textbf{(2-33)}$$

A cubic packing arrangement (Fig. 17) of spheres has a porosity of 0.48. Therefore, the proppant pack volume in the fracture, V_{frac}, is:

$$V_{prop} = V_{frac}\ (1 - \emptyset) \quad \textbf{(2-34)}$$

$$1.208\ \text{cm}^3 = V_{frac}\ (1 - 0.48) \quad \textbf{(2-35)}$$

$$V_{frac} = 2.323\ \text{cm}^3 \quad \textbf{(2-36)}$$

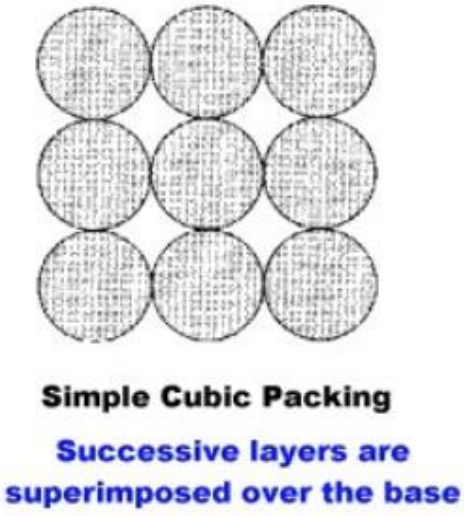

Fig. 17 – Cubic packing arrangement

The fracture surface has a surface area of 10 in^2. Converting it to metric units:

$$A = 10\ \text{in}^2 \left(\frac{2.54\ \text{cm}}{1\ \text{in.}}\right)^2 = 64.5\ \text{cm}^2 \quad \textbf{(2-37)}$$

The propped fracture volume V_{frac} is the fracture surface area multiplied by the height of the proppant pack. In a monolayer proppant pack, the proppant pack height is equal to the diameter d_p of a proppant grain. In a multilayer pack, the proppant pack height is the product of d_p and the number of proppant layers. Therefore the proppant pack height d_p using 3.2 grams of proppant is:

$$V_{frac} = d_p A \quad \textbf{(2-38)}$$

$$2.323\ \text{cm}^3 = d_p(64.5\ \text{cm}^2) \quad \textbf{(2-39)}$$

$$d_p = 0.036\ \text{cm} \quad \textbf{(2-40)}$$

The height of the proppant pack d_p is 0.036 cm. Since 0.036 cm is less than the proppant diameter of 0.045 cm this is less than a full monolayer, a partial monolayer proppant pack. The number of proppant layers at 0.1 lb/ft^2 concentration is:

$$\#\ \text{layers} = \frac{d_p}{diameter_{prop}} \quad \textbf{(2-41)}$$

$$\#\ \text{layers} = \frac{0.036\ \text{cm}}{0.045\ \text{cm}} = 0.8\ \text{layers} \quad \textbf{(2-42)}$$

Therefore

$$3.2\ \text{grams} = 0.8\ \text{layers} \quad \textbf{(2-43)}$$

The number of proppant layers at 0.2 lb/ft^2 concentration is twice that or 1.6 layers.

$$6.4\ \text{grams} = 1.6\ \text{layers} \quad \textbf{(2-44)}$$

Fig. 18 shows the two proppant concentrations distributed on a fracture surface and Fig. 19 shows up-close photos of the partial monolayer proppant pack at 0.1 lb/ft^2 and pack at 0.2 lb/ft^2.

(a)

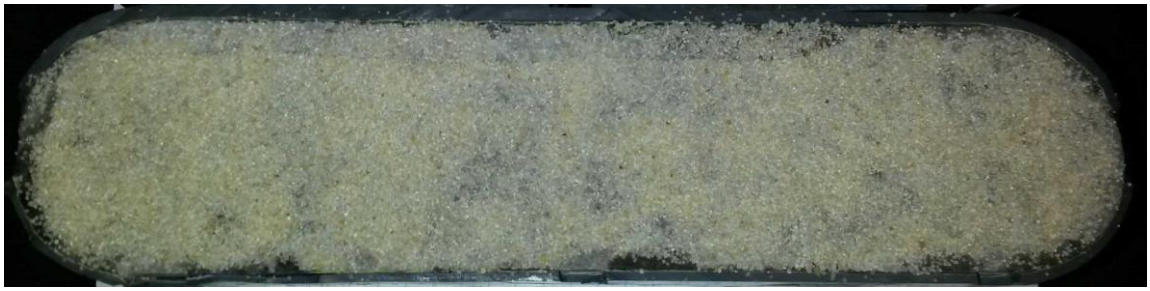

(b)

Fig. 18a, b – Proppant distributions at 0.1 lb/ft^2 and 0.2 lb/ft^2

(a) (b)

Fig. 19a, b – Up-close photos of partial monolayer and multilayer proppant packs

2.9 Experimental design matrix and conditions

In order to analyze the behavior of conductivity within a section of single horizontal well, samples were collected at locations approximately 150 feet apart along a 1,015 lateral length of the outcrop. Only artificially induced, aligned fractures were used in this study. Conductivity experiments were performed on each sample in three different trials: unpropped, and 0.1 lb/ft^2 and 0.2 lb/ft^2 concentrations of proppant. Only 30/50 mesh white sand was used as proppant. Gas flow rates were kept below 2 liters per minute during experiments in order to minimize the effects of turbulent flow. High gas flow rates cause the flow type to change from laminar to turbulent flow. In turbulent flow, the Forchheimer equation must be used to calculate conductivity.. However, the low flowrates used during experiments reducing it to Darcy's equation.

In addition, profilometer surface scans were performed on two samples before and after conductivity tests in order to identify permanent alterations in the fracture surface. These alterations can modify pre-existing flow channels through the fracture and decrease the conductivities.

Finally, FTIR was performed on each of the seven samples to determine their mineralogical composition. This testing was outsourced to a commercial laboratory. The percentages of carbonate, quartz, clay, and feldspar in each sample were identified to determine if there was a significant variance in mineral content. Fig. 20 displays a work flow chart for this study.

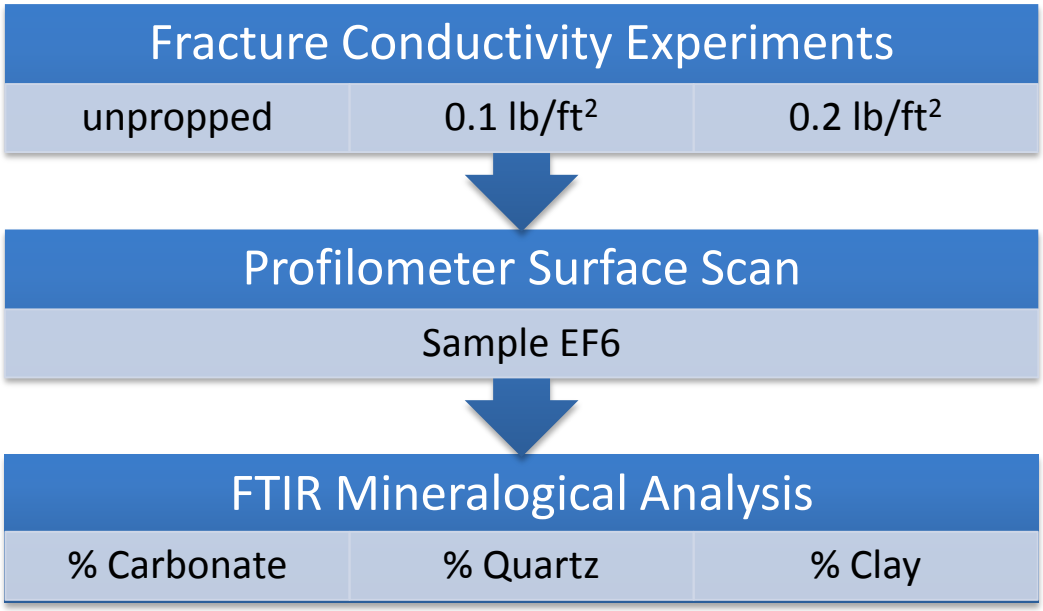

Fig. 20 - Work progression flow chart

2.10 Induced fractures

At a commercial masonry shop, fractures were artificially induced in the lab samples along the natural bedding planes. This created rough aligned fracture surfaces with surface profiles that were unique in each sample. A graphic of an unpropped fracture appears in Fig. 21. The samples arrived taped closed from the masonry shop, and were left closed during sample preparation and unpropped conductivity testing. When the fractures were first opened to insert sand for propped experiments, no loose infill material was found in any of the fractures. Proppant was manually placed in the fracture, resulting in a side profile similar to the graphic in Fig. 22.

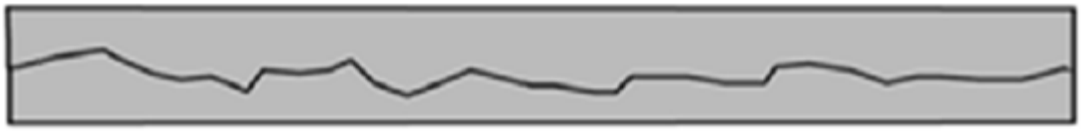

Fig. 21 – Unpropped aligned fracture graphic

Fig. 22 – Propped aligned fracture graphic

2.11 Rock properties

Mineral composition and fracture surface profiles were chosen as additional tests due to their relationship with fracture conductivity. Mineralogical composition affects the brittleness of a rock by its influence on two rock mechanical properties, Young's Modulus and Poisson's Ratio. A high Young's Modulus and low Poisson's Ratio indicates that a rock is ductile. Ductile shale is not a preferred reservoir rock because of its proclivity to close hydraulic fractures, due to the potential for proppant embedment in the fracture surface (Clemons et al., 2013).

Profilometer scans of the fracture surfaces were of interest because they shed light on permanent changes in the surface profile caused by the applied closure stress during conductivity experiments. Since these alterations can change the profile of flow channels through the fracture, they were of significant interest due to their potential effect on conductivity. Scans were performed on sample EF6 before and after

unpropped and propped conductivity experiments in order to closely evaluate this variable.

3. EXPERIMENTAL RESULTS AND DISCUSSION

3.1 Experimental and analytical overview

The seven Eagle Ford Shale samples, labeled EF1 through EF7, were used to conduct a series of fracture conductivity experiments, mineral composition analyses, and surface profile scans. In order to maintain the consistency of experimental results, the same seven samples were used throughout all experiments. Three types of conductivity experiments were performed in a consecutive manner on all seven samples, the order of which is as follows: unpropped, propped with 0.1 lb/ft^2 of 30/50 mesh white sand, and propped with 0.2 lb/ft^2 of 30/50 mesh white sand. Unpropped fracture conductivity was measured at closure stresses between 1,000 psi and 4,000 psi at 1,000 psi increments. The unpropped experiments were limited to a maximum closure stress of 4,000 psi because the flow of nitrogen gas through the fracture is almost completely blocked above this closure stress and conductivity measurements rapidly approach zero. Propped fracture conductivity experiments at proppant concentrations of 0.1 lb/ft^2 and 0.2 lb/ft^2 were measured at closure stresses between 1,000 psi and 6,000 psi at 1,000 psi increments. Propped experiments were limited to a maximum closure stress of 6,000 psi because this is generally the highest formation closure stress in the Eagle Ford Shale (Centurion, 2011).

The analysis of the experimental conductivity results is performed in two segments. First, the conductivity data sets of the seven samples within each experiment type are compared; section 3.2 evaluates the conductivity of unpropped fractures, section 3.3.1 evaluates the conductivity of fractures propped with 0.1 lb/ft^2 sand concentration,

and section 3.3.2 evaluates the conductivity of fractures propped with 0.2 lb/ft^2 sand concentration. Secondly, the results of the three experiment types are compared to each other in section 3.4 in order to evaluate the effect of proppant concentration on fracture conductivity.

In addition to conductivity experiments, the mineral composition of each sample that was determined by Fourier transform infrared analysis is presented in section 3.5. Finally, surface profile scans of sample EF6 that were performed before and after conductivity experiments and are presented in section 3.6. The high compressive forces applied to the samples by the load frame can potentially create permanent alterations to the fracture surface profiles and change the system of flow channels through the fracture. Since this alteration in profile could skew conductivity measurements in subsequent experiments, these scans were performed to investigate its effect, if any.

3.2 Conductivity of unpropped fractures

The conductivity of unpropped fractures relies solely on disparities between the fracture surface profiles of the two sample sections to create flow channels. The measurements reflect the influence of unpropped fracture width and permeability on conductivity. The unpropped experiments also provide baseline measurements to compare to the conductivity of propped fractures. In the following graphs, the y-axis of conductivity is plotted on a logarithmic scale because the high variation between values is more easily displayed in this manner than on a linear scale. Fig. 23 is a graph of the unpropped fracture conductivity values of the seven lab samples.

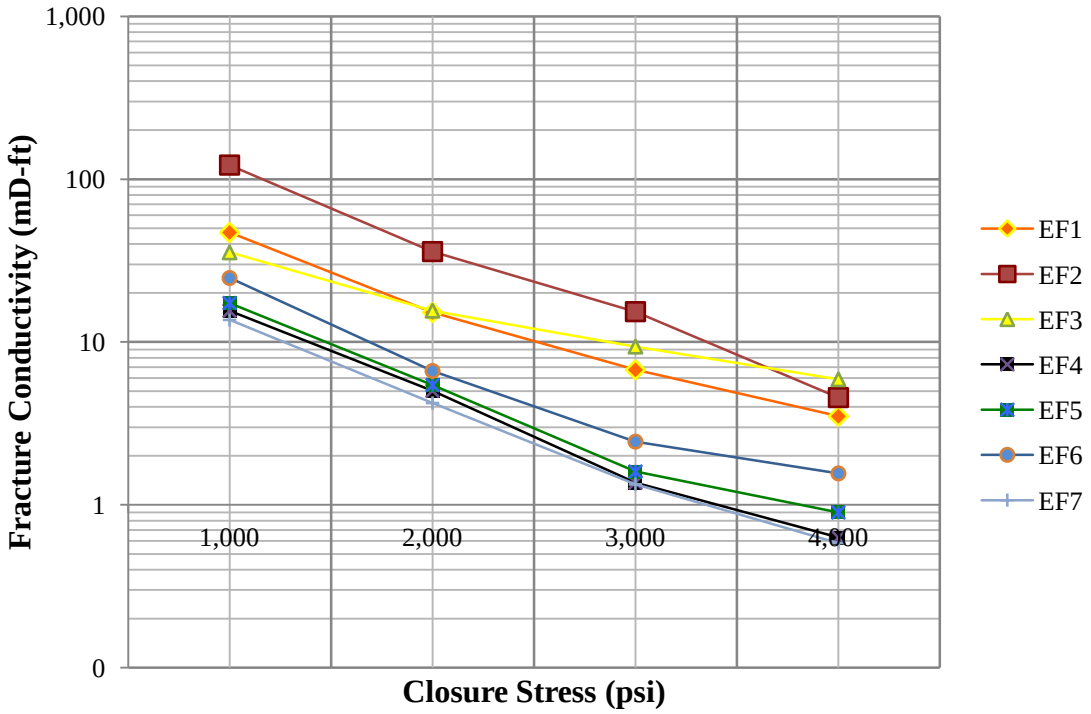

Fig. 23 – Conductivity of unpropped fractures

Fig. 23 shows that the results of seven unpropped conductivity experiments have similar trends. The conductivity values in each experiment appear to decrease at similar rates as closure stress increases. The seven conductivity values at each closure stress are all within the same order of magnitude, and the values decrease from an average of 38 mD-ft at 1,000 psi to an average of 2 mD-ft at 4,000 psi. The variation between conductivity values at each closure stress is attributed to the difference in rough fracture surface profiles between samples, which create different systems of flow channels through the samples' unpropped fractures.

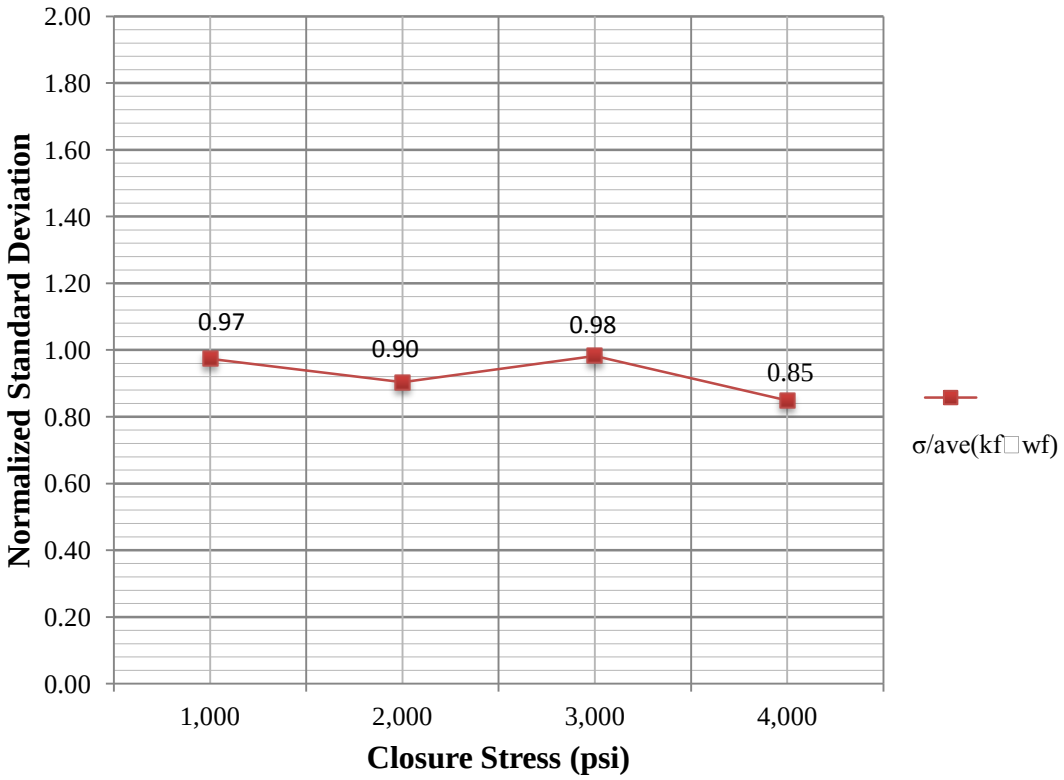

Fig. 24 – Normalized standard deviation of unpropped conductivity values

Fig. 24 shows the normalized standard deviation of unpropped fracture conductivity values at each closure stress. Normalized standard deviation is calculated by dividing the standard deviation σ of the seven conductivity values at a given closure stress by the average $[ave(k_f w_f)]$ of those seven conductivity values. This method of analysis allows for a more accurate comparison than the by comparing the standard deviation values at each closure stress.

Fig. 24 shows that there is minimal variation between the results of the unpropped experiments on samples EF1 through EF7 as closure stress increases.

3.3 Conductivity of propped fractures

After the completion of unpropped conductivity experiments, propped experiments were performed with 30/50 mesh white sand. Proppant was manually poured and evenly distributed on the fracture surfaces. Two different sand concentrations, 0.1 lb/ft^2 and 0.2 lb/ft^2, were used to study the effect of proppant concentration on fracture conductivity. The results also provide an opportunity to evaluate the effects of a partial monolayer and multilayer proppant packs on conductivity. Propped experiments were limited to a maximum of 6,000 psi closure stress because this is generally the upper limit of closure stress noted in horizontal well logs in the Eagle Ford Shale.

In order to isolate the effect of proppant concentration on conductivity, the same proppant size and type were used for all propped experiments. Nevertheless, several proppant variables that cannot be controlled inevitably contribute to variation in conductivity measurements. Proppant crushing, embedment in the fracture surface, and localized distributions due to surface asperities are examples of those uncontrollable factors.

3.3.1 Conductivity measurements at 0.1 lb/ft^2 concentration

Fig. 25 is a graph of the propped fracture conductivity values of the seven samples using a concentration of 0.1 lb/ft^2 30/50 mesh white sand. At 0.1 lb/ft^2 concentration, proppant concentration is a partial proppant monolayer of 0.8 layers.

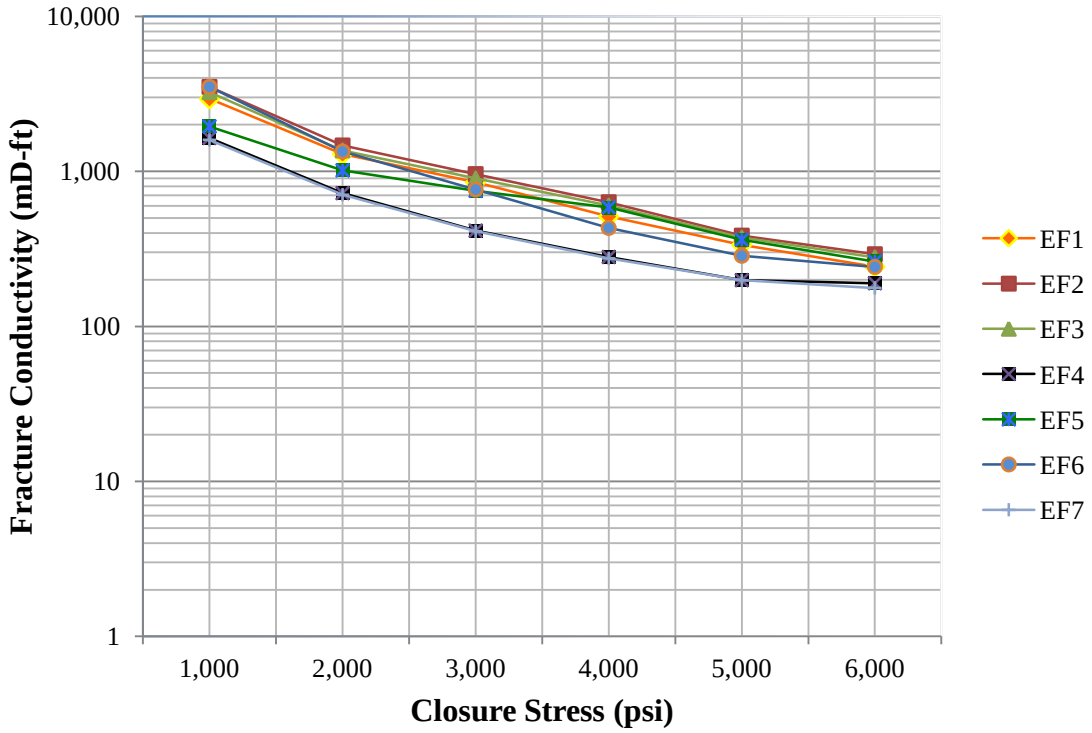

Fig. 25 – Conductivity of propped fractures at 0.1 lb/ft^2 concentration

Fig. 25 shows that the results of the seven conductivity experiments at 0.1 lb/ft^2 proppant concentration are similar. The seven conductivity datasets decrease at similar rates as closure stress increases. Conductivity values at each closure stress are also within the same order of magnitude, and decrease from an average of 2,717 mD-ft at 1,000 psi to an average of 236 mD-ft at 6,000 psi.

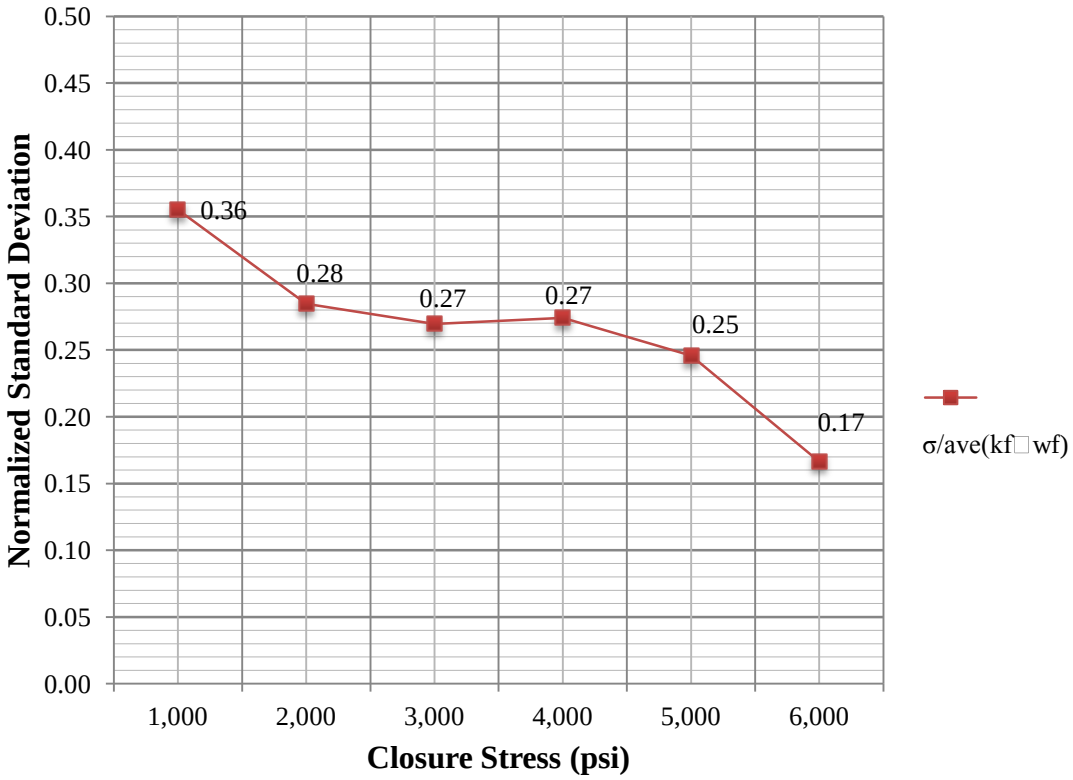

Fig. 26 - Standard deviation of propped conductivity values at 0.1 lb/ft^2

Fig. 26 shows that there is minimal variation between the results of the propped experiments on samples EF1 through EF7. There is a decreasing trend in normalized standard deviation as closure stress increases from 1,000 psi to 6,000 psi. This converging trend in variation is primarily attributed to the settling of the proppant pack as closure stress increases; an unsettled proppant pack is likely to result in a wider variety of fracture widths and permeabilities, thereby varying conductivity values.

3.3.2 Conductivity measurements at 0.2 lb/ft^2 concentration

Fig. 27 is a graph of the propped conductivity values of the seven samples using a proppant concentration of 0.2 lb/ft^2 30/50 mesh white sand. At 0.2 lb/ft^2 proppant concentration, proppant concentration is 1.6 layers, slightly more than a complete proppant monolayer.

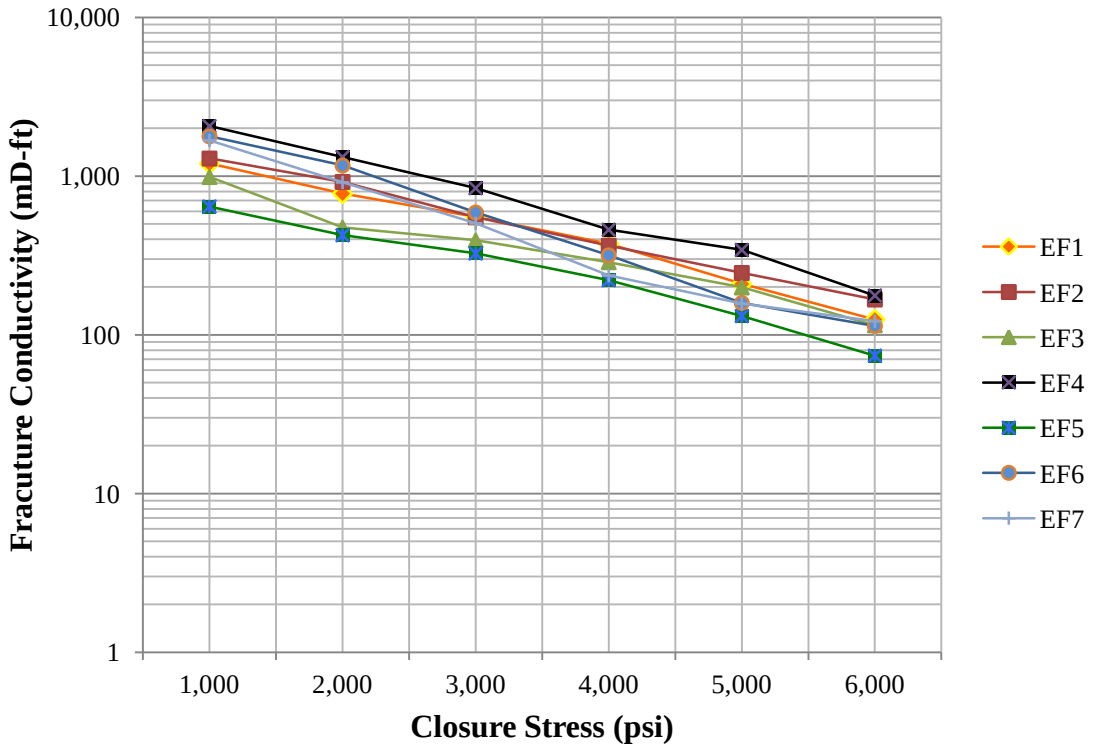

Fig. 27 – Conductivity of propped fractures at 0.2 lb/ft^2 concentration

Fig. 27 shows that the results of the seven propped experiments performed at 0.2 lb/ft^2 concentration are similar. Conductivity values at each closure stress are within the

same order of magnitude, and decrease from an average of 1,380 mD-ft at 1,000 psi to an average of 140 mD-ft at 6,000 psi.

Fig. 28 is a graph of the normalized standard deviation between the conductivity values at 0.2 lb/ft^2 proppant concentration.

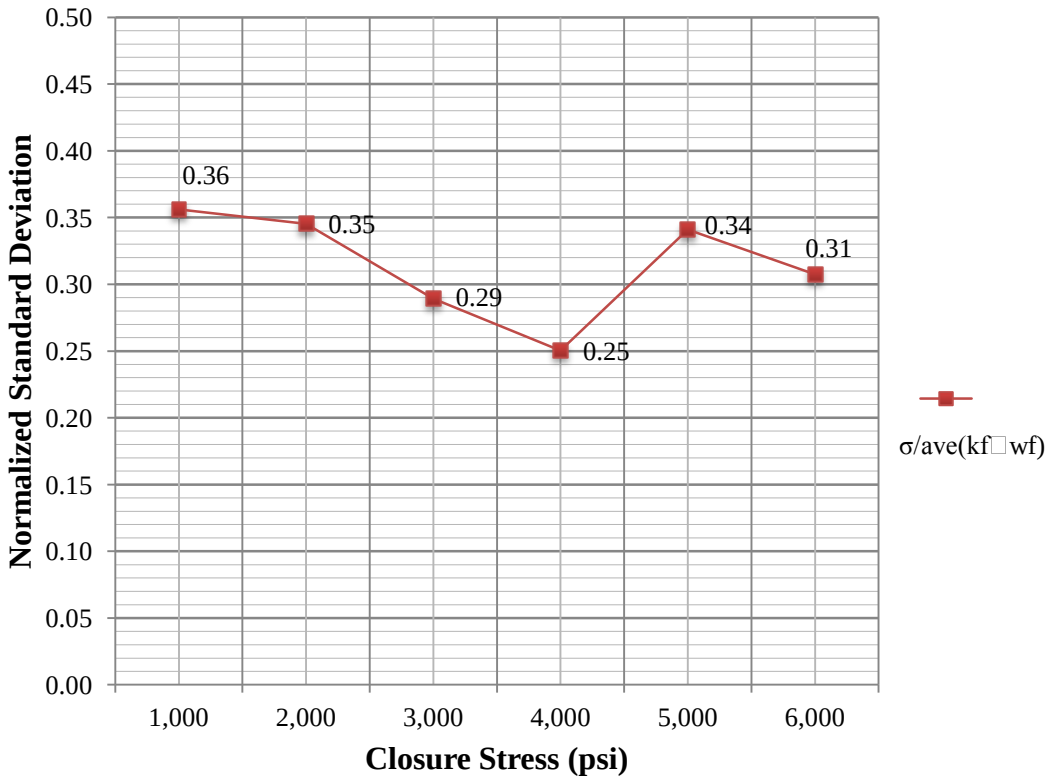

Fig. 28 - Standard deviation between conductivity values at 0.2 lb/ft^2

Fig. 28 shows that there is again minimal variation between the results of the propped experiments of 0.2 lb/ft^2 on samples EF1 through EF7.

3.4 Comparison of conductivity of the three experiment types

Within each of the three experiment types, the results of all twenty-one conductivity experiments were plotted graphically in order to compare them (Fig. 29).

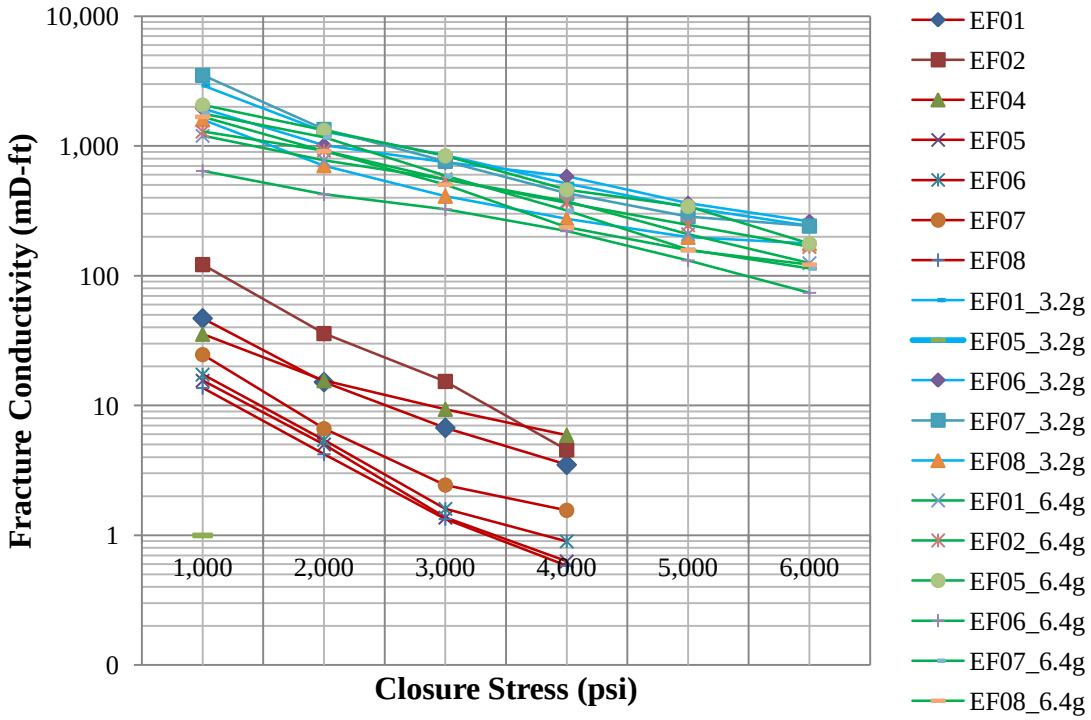

Fig. 29 – Results of twenty-one conductivity experiments

Fig. 29 shows that the experimental results of the propped experiments at 0.1 lb/ft^2 and 0.2 lb/ft^2 are approximately two orders of magnitude greater than the unpropped experiments. The higher conductivity of the propped experiments is due to proppant creating a higher fracture permeability k_f and a greater fracture width w_f than the unpropped experiments. Fig. 29 also shows that the 0.1 lb/ft^2 experiments overlap

with the results of the 0.2 lb/ft^2 experiments. This overlap shows that fracture conductivity is quite similar at either of these proppant concentrations.

Within each of the three experiment types, the seven conductivity measurements were averaged at each closure stress in order to evaluate the effects of proppant concentration on fracture conductivity. A graph of the average conductivity values is shown in Fig. 30 and the equations of exponential trend lines fit to each of the semi-log datasets are also displayed.

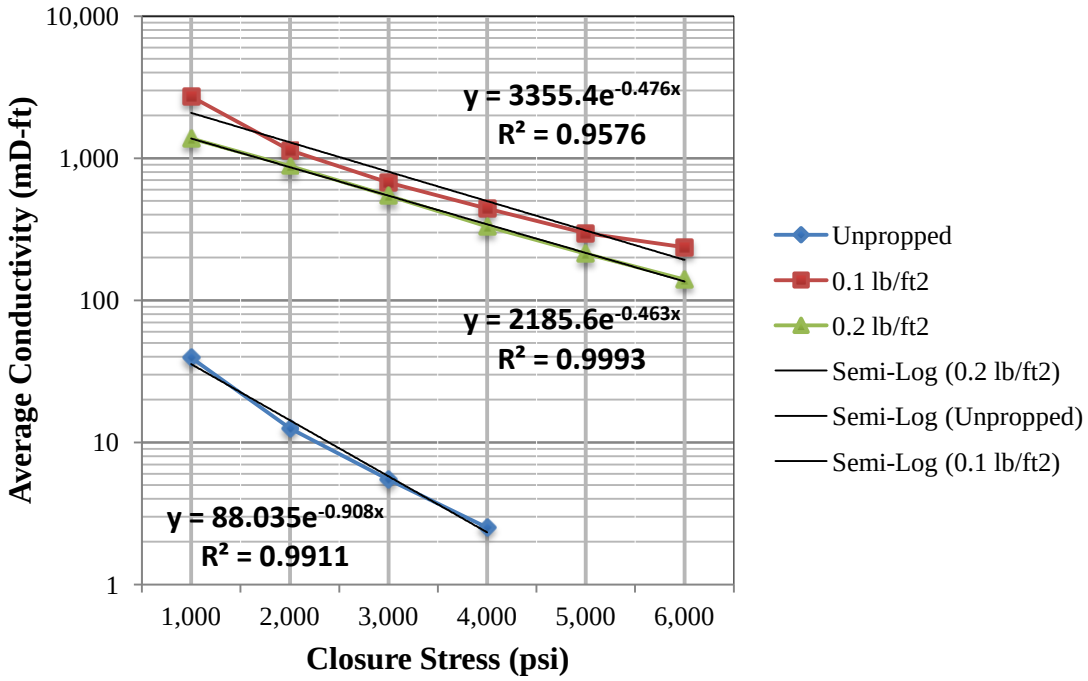

Fig. 30 – Average fracture conductivity values of the three experiment types

Fig. 30 shows that the conductivity values at 0.1 lb/ft^2 proppant concentration are on average 49% greater than the values at 0.2 lb/ft^2 concentration; this calculation

appears in Appendix C. The higher conductivity values at 0.1 lb/ft^2 can be attributed to the effects of a partial monolayer pack at 0.1 lb/ft^2 and a multilayer proppant pack of 1.6 layers at 0.2 lb/ft^2; the partial proppant monolayer creates a propped fracture width that has conductivity values quite similar to the conductivity of a proppant pack composed of 1.6 layers, as suggested by Darin and Huitt (1959). However, the partial monolayer pack has greater porosity than a 1.6 layer proppant pack due to the open spaces between proppant particles.

The exponential equations shown in Fig. 30 are expressed in the form $N = N_o e^{-\lambda t}$. The decay constant λ is a measure of how rapidly the conductivity is decreasing in each of the three experiment types; the slope of the line is the negative of the decay constant. R^2 is a measure of how accurate the model is; the closer R^2 is to 1, the more accurate the model. Table 3 below lists the decay constants and R^2 values.

	Decay Constant λ (psi^{-1})	**R^2 Value**
Unpropped	0.908	0.991
0.1 lb/ft^2	0.476	0.958
0.2 lb/ft^2	0.463	0.999

Table 3 – Decay constants and R^2 values for 3 experiment types

The decay constants in Table 3 have a decreasing trend with increasing proppant concentration; therefore with greater proppant concentrations up to a full monolayer, conductivity decreases at a slower rate as closure stress increases from 1,000 to 6,000 psi. This trend suggests that fractures with higher proppant concentrations are more

resistant to the flow inhibiting effects of high closure stresses. The denser proppant pack at 0.2 lb/ft^2 may be resulting in shallower proppant embedment and less proppant crushing, since there are twice as many proppant particles to support the closure stress.

The three R^2 values are all very close to 1, so the models are thought to be quite accurate. This statistical value gives a level of validity to the conclusions made in this section.

3.5 Mineralogical data

Fig. 31 shows the mineral composition of each sample that was determined by FTIR.

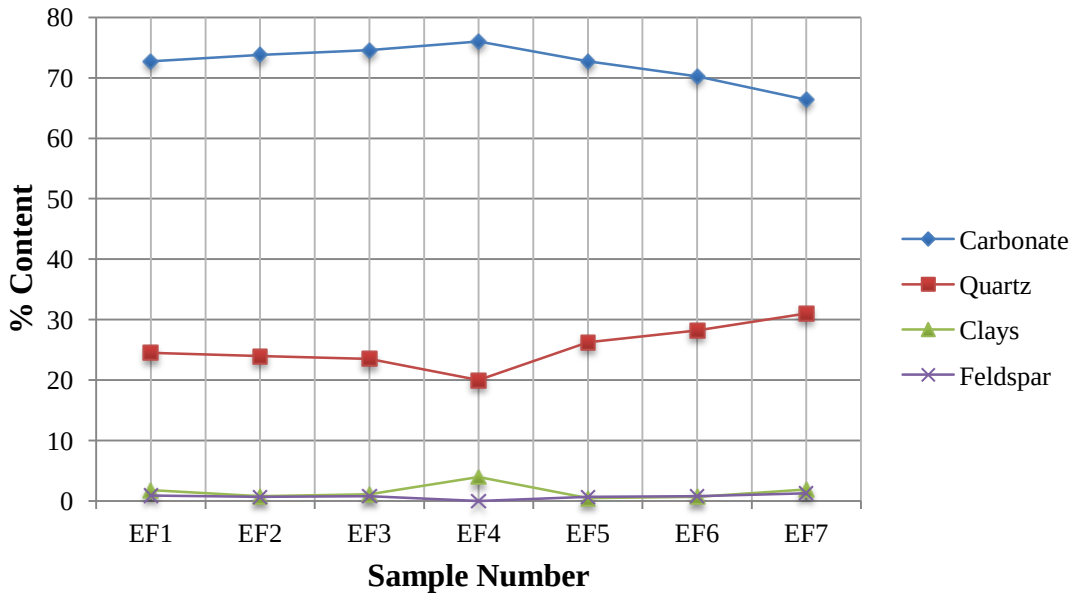

Fig. 31 – Mineral composition of the seven lab samples

The mineral composition is generally similar across the sampling length. The average composition of clay, carbonate, quartz, and feldspar in each sample is 2%, 72%, 20%, and 3%, respectively. This suggests that the variation of conductivity measurements between samples EF1 through EF7 is not caused principally by a difference in geomechanical properties, which are a function of mineral composition (Clemons et al., 2013). Therefore, the minimal variation in conductivity values between samples EF1 through EF7 may be caused by different proppant distributions within the fractures of the seven lab samples, a result of the peaks and valleys that are unique to each rough fracture surface.

3.6 Surface profile scans

Surface profile scans were performed on sample EF6 before and after a closure stress of 4,000 psi was applied during the unpropped experiment. The results displayed in Fig. 32 and Fig. 33 show that a 4,000 psi closure stress causes permanent alteration to the fracture surface profile.

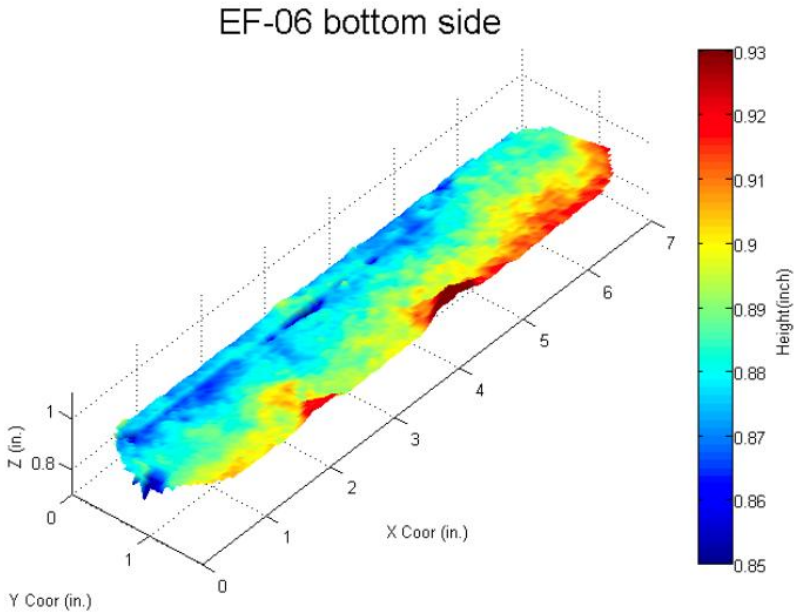

Fig. 32 – Surface profile scan before 4,000 psi closure stress

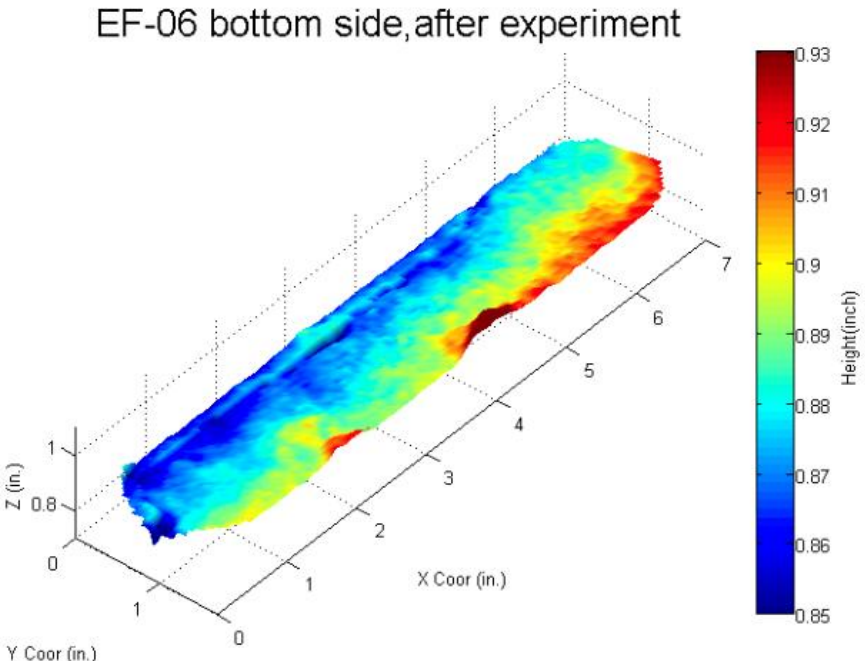

Fig. 33 – Surface profile scan after 4,000 psi closure stress

The scans show that the surface of the lab sample is permanently compacted by up to 0.02 inches in depth by the closure stress. These results show that the Eagle Ford lab samples are subject to permanent deformation during experiments. This deformation could potentially be a source of error in the results of consecutive conductivity experiments performed on the same lab sample.

4. CONCLUSION AND RECOMMENDATIONS

4.1 Conclusions

This study evaluated several properties of Eagle Ford Shale samples collected from a short horizontal length of a facies B outcrop. The primary goal was to investigate the relationship between fracture conductivity and proppant concentration. The examination of mineral composition and surface profile scans were performed as a secondary means of analysis in order to identify geological factors that could potentially contribute to the variations in fracture conductivity.

The following conclusions are made based on the fracture conductivity experiments:

1. Propped fracture conductivity values at 0.1 lb/ft^2 and 0.2 lb/ft^2 are approximately two orders of magnitude higher than unpropped conductivity values. These results show that fracture conductivity in the Eagle Ford Shale is significantly increased even by the low proppant concentrations of a partial monolayer pack and proppant pack of 1.6 layers.
2. Propped conductivity values at 0.1 lb/ft^2 proppant concentration are on average 49% higher than measurements at 0.2 lb/ft^2 concentration. This difference is attributed to the effects of a partial monolayer pack at 0.1 lb/ft^2 and a 1.6 layer proppant pack at 0.2 lb/ft^2; since propped fracture width is almost equal at 0.1 lb/ft^2 and 0.2 lb/ft^2 concentrations, the 1.6 layer proppant pack provides less permeability than a partial monolayer proppant pack.

3. As closure stress increases, propped fracture conductivity values at 0.1 lb/ft^2 proppant concentration decrease more rapidly than values at 0.2 lb/ft^2 concentration. These results show that a partial monolayer is less resistant to the flow inhibiting effects caused by high closure stresses, due to their lower areal concentration. Deeper proppant embedment and greater proppant crushing may be occurring in the partial monolayer as closure stress increases.

The results of the FTIR scans show that the mineral contents of the Eagle Ford samples do not vary notably across the sampling length. Therefore, the slight lateral variations in fracture conductivity between samples at each proppant concentration is not likely due to differences in mineral content. Rather, the variations in conductivity can be attributed to the differences in proppant packs within the lab samples, a result of the peaks and valleys that are unique to each of the fracture surfaces of the lab samples, EF1 through EF7.

The surface scans show that the rock surface profile is permanently altered by the high closure stresses applied during the unpropped conductivity experiments. The crushing of surface asperities changes the network of flow channels through the fracture surface. Therefore, this alteration is potentially a source of error in the consecutive experiments performed on the lab samples.

4.2 Recommendations

Future work should investigate the conductivity of lab samples using proppant concentrations greater than 0.2 lb/ft^2 concentration. In addition, conductivity

experiments performed with different concentrations of a partial proppant monolayer could provide more evidence to validate Darin and Huitt's partial proppant monolayer theory, in this case with actual lab samples. Performing conductivity experiments with mineral oil instead of dry nitrogen gas is another potential area of future work that could contribute to the understanding of the different reservoir fluid zones in the Eagle Ford Shale.

REFERENCES

Brannon, H. D., Malone, M. R., Richards, A. R., Wood, W. D., Edgeman, J. R., Bryant J. L. (2004). Maximizing Fracture Conductivity with Proppant Partial Monolayers: Theoretical Curiosity or Highly Productive Reality? SPE Annual Technical Conference and Exhibition. Houston, Texas. SPE-90698-MS.

Centurion, S. M. (2011). Eagle Ford Shale: A Multistage Hydraulic Fracturing, Completion Trends and Production Outcome Study Using Practical Data Mining Techniques. SPE Eastern Regional Meeting, Colombus, Ohio. SPE-149258-MS.

Clemons, K., Bodziak, R., Stephens, A., Meek, R. (2013). Leveraging Seismic Attributes to Understand the Frac-Able Limits and Reservoir Performance in the Eagle Ford Shale, South Texas, USA. Unconventional Resources Technology Conference. Denver, Colorado. SPE-168740-MS.

Diomampo, G., Chen, C. Y., Li, K., Horne, R. N. (2001). Relative Permeability Through Fractures. In Proc. 27 the Workshop on Geothermal Reservoir Engineering, 28-30. SGP-TR-170.

Economides, M.J., Hill, D.A., Ehlig-Economides, C., Zhu, D. (2012). Petroleum Production Systems, Second Edition. Englewood Cliff, N.J. PTR Prentice Hall, 2012. ISBN: 0-13-703158-0.

Gardner, R., Pope, M. C., Wehner, M. P., Donovan, A. D. (2013). Comparative Stratigraphy of the Eagle Ford Group Strata in Lozier Canyon and Antonio Creek, Terrell County, Texas. GCAGS Journal 2(1): 42-52.

Gidley, J. L. (1989). Recent Advances in Hydraulic Fracturing. SPE Monograph Volume 12, 1989. ISBN: 1-55563-020-0.

Hill, A. D., Zhang, J., Zhu, D., Kamenov, A. N. (2013). Laboratory Measurement of Hydraulic Fracture Conductivities in the Barnett Shale. International Petroleum Technology Conference. Bejing, China. IPTC-16444-MS.

Jambhekar, V. A. (2011). Forchheimer Porous-Media Flow Models - Numerical Investigation and Comparison with Experimental Data. Doctoral dissertation, University of Stuttgart. Stuttgart, Germany. Matrikelnummer 2550192.

Kamenov, A., Zhu, D., Hill, A. D., Zhang, J. (2013). Laboratory Measurement of Hydraulic Fracture Conductivities in the Barnett Shale. SPE Hydraulic Fracturing Technology Conference. The Woodlands, Texas. SPE-163839-MS.

Mayerhofer, M. J., Richardson, M. F., Walker, R. N., Meehan, D. N., Oehler, M. W., Browning, J. J. (1997). Proppants? We Don't Need No Proppants. SPE Annual Technical Conference. San Antonio, Texas. SPE-38611-MS.

Montgomery, C. T., Smith, M. B. (2010). History of Fracturing: An Enduring Technology. Journal of Petroleum Technology 1(1): 26-28.

Mullen, J. (2010). Petrophysical Characterization of the Eagle Ford Shale in South Texas. Canadian Unconventional Resources and International Petroleum Conference. Calgary, Alberta, Canada. SPE-138145-MS.

Palisch, T. T., Vincent, M. C., Handren, P. J. (2008). Slickwater Fracturing – Food for Thought. SPE Annual Technical Conference. Denver, Colorado. SPE-115766-PA.

Quirein, J., Praznik, G., Galford, J., Chen, S. Murphy, E. Witkowski, J. (2013). A Workflow to Evaulate Mineralogy, Porosity, TOC, and Hydrocarbon Volume in the Eagle Ford Shale. Unconventional Resources Conference and Exhibition. Brisbane, Australia. SPE-167012-MS.

Rivers, M., Zhu, D., Hill, A. D. (2012). Proppant Fracture Conductivity With High Proppant Loading and High Closure Stress. SPE Hydraulic Fracturing Technology Conference. The Woodlands, Texas. SPE-151972-MS.

Sahoo, A. K., Mukherjee, D., Mukherjee, A., Srivastava, M. (2013). Reservoir Characterization of Eagle Ford Shale through Lithofacies Analysis for Identification of Sweet Spot and Best Landing Point. Unconventional Resources Technology Conference. Denver, Colorado. SPE-168677-MS.

Shelley, R. F., Saugier, L. D., Al-Tailji, W., Guliyev, N., Shah, K. (2012). Understanding Hydraulic Fracture Stimulated Horizontal Eagle Ford Completions. SPE/EAGE European Unconventional Resources Conference and Exhibition. Vienna, Austria. SPE-152533-MS.

Stegent, N. A., Wagner, A. L., Mullen, J. Borstmayer, R. E. (2010). Engineering a Successful Fracture-Stimulation Treatment in the Eagle Ford Shale. SPE Tight Gas Completions Conference. San Antonio, Texas. SPE-136183-MS.

US Energy Information Administration (US EIA) (2013). Technically Recoverable Shale Oil and Shale Gas Resources: An Assessment of 137 Shale Formations in 41 Countries Outside the United States. US Department of Energy, Washington, DC.

Viswanathan, A. V., Altman, R. M., Oussoltsev, D., Kanneganti, K. T., Xu, J., Grant, D., Indriati, S., Pena, A. A., Loayza, M. P., Kirkham, B., Rhein, T. K. (2011). Completion Evaluation of the Eagle Ford Formation with Heterogeneous Proppant Placement. Canadian Unconventional Resources Conference. Calgary, Alberta, Canada. SPE-149390-MS.

Walker, R. N., Hunter, J. L., Brake, A. C., Fagin, P. A., Steinsberger, N. (1998). Proppants, We Still Don't Need No Proppants – A Perspective of Several Operators. SPE Annual Technical Conference. New Orleans, Louisiana. SPE-49106-MS.

Wendorff, C. L., Alderman, E. N. (1969). Prop-Packed Fractures – A Reality on Which Productivity Increase Can be Predicted. SPE Rocky Mountain Regional Meeting. Denver, Colorado. SPE-2452-MS.

Zhou, D., Zhang, G., Ruan, M., He, A., Wei, D. (2011). Comparison of Fracture Conductivities from Field and Lab. International Petroleum Technology Conference. Bangkok, Thailand. IPTC-14706-MS.

APPENDIX A

RESULTS OF THE FRACTURE CONDUCTIVITY EXPERIMENTS

		EF1	EF2	EF3	EF4	EF5	EF6	EF7
unpropped	Clo. Stress (psi)	k_f-w_f (md-ft)	k_f-w_f (md-ft)	k_f-w_f (md-ft)	k_f-w_f (md-ft)	k_f-w_f (md-ft)	k_f-w_f (md-ft)	k_f-w_f (md-ft)
	1,000	47.1	122.1	35.5	15.6	17.3	24.7	13.7
	2,000	15.2	35.9	15.6	5.0	5.4	6.6	4.2
	3,000	6.8	15.4	9.4	1.4	1.6	2.4	1.3
	4,000	3.5	4.6	5.9	0.6	0.9	1.6	0.6

		EF1	EF2	EF3	EF4	EF5	EF6	EF7
0.1 lb/ft^2 30/50 mesh sand	Clo. Stress (psi)	k_f-w_f (md-ft)	k_f-w_f (md-ft)	k_f-w_f (md-ft)	k_f-w_f (md-ft)	k_f-w_f (md-ft)	k_f-w_f (md-ft)	k_f-w_f (md-ft)
	1,000	2,936	3,705	3,683	1,642	1,947	3,508	1,597
	2,000	1,292	1,487	1,398	723	1,014	1,343	706
	3,000	850	778	753	415	750	763	411
	4,000	511	515	502	280	584	432	274
	5,000	336	375	319	198	362	285	198
	6,000	242	287	252	190	262	242	177

		EF1	EF2	EF3	EF4	EF5	EF6	EF7
0.2 lb/ft^2 30/50 mesh sand	Clo. Stress (psi)	k_f-w_f (md-ft)	k_f-w_f (md-ft)	k_f-w_f (md-ft)	k_f-w_f (md-ft)	k_f-w_f (md-ft)	k_f-w_f (md-ft)	k_f-w_f (md-ft)
	1,000	1,200	1,292	998	2,067	644	1,780	1,680
	2,000	777	920	639	1,320	425	1,167	914
	3,000	554	551	445	840	326	591	505
	4,000	375	365	337	460	221	317	237
	5,000	209	246	245	343	132	159	157
	6,000	125	167	198	177	74	114	122

APPENDIX B

		Analysis of 7 kf-wf Values at Each Closure Stress		
	Clo. Stress (psi)	Std. Dev. σ (md-ft)	Average k_f-w_f (md-ft)	σ / Ave(k_f-w_f)
unpropped	1,000	38.4	39.4	0.97
	2,000	11.4	12.6	0.90
	3,000	5.4	5.5	0.98
	4,000	2.1	2.5	0.85

		Analysis of 7 kf-wf Values at Each Closure Stress		
	Clo. Stress (psi)	Std. Dev. σ (md-ft)	Average k_f-w_f (md-ft)	σ / Ave(k_f-w_f)
0.1 lb/ft^2 30/50 mesh sand	1,000	964.8	2,717	0.36
	2,000	323.7	1,138	0.28
	3,000	181.8	674	0.27
	4,000	121.3	443	0.27
	5,000	72.8	296	0.25
	6,000	39.3	236	0.17

		Analysis of 7 kf-wf Values at Each Closure Stress		
	Clo. Stress (psi)	Std. Dev. σ (md-ft)	Average k_f-w_f (md-ft)	σ / Ave(k_f-w_f)
0.2 lb/ft^2 30/50 mesh sand	1,000	491.6	1,380	0.36
	2,000	304.0	880	0.35
	3,000	157.5	544	0.29
	4,000	82.7	330	0.25
	5,000	72.6	213	0.34
	6,000	42.9	140	0.31

Statistical analysis of conductivity data

APPENDIX C

Closure Stress (psi)	$\frac{Ave(k_f w_f) \text{ @ } 0.1\ lb/ft^2}{Ave(k_f w_f) \text{ @ } 0.2\ lb/ft^2}\ x\ 100$
1,000	196.9%
2,000	129.2%
3,000	123.8%
4,000	134.1%
5,000	139.1%
6,000	169.1%
Average of six values →	**148.7%**

Calculation of % increase in conductivity values between 0.1 lb/ft^2 proppant concentration and and 0.2 lb/ft^2 proppant concentration.

APPENDIX D

			Rate (bpm)		Clean Volume (gallons)		Slurry Volume	Proppant (Sacks)			Prop Conc. (lb/gal @ Blender)	
	Stage Name	Description	CLEAN	DIRTY	STAGE	JOB	STAGE	STAGE	REMAIN	PUMPED	START	END
1	Load Well	Treated Water	10.0	10	10000	10000	10000					
2	15% HCl Acid	15% HCl Acid	10.0	10	2000	12000	2000					
3	Pad	Treated Water	60.0	60	25000	37000	25000					
4	0.50 ppg 100 Mesh	Treated Water	58.7	60	10000	47000	10228	50	3553	50	0.50	0.50
5	0.75 ppg 100 Mesh	Treated Water	58.0	60	7000	54000	7239	53	3500	103	0.75	0.75
6	1.00 ppg 100 Mesh	Treated Water	66.9	70	10000	64000	10456	100	3400	203	1.00	1.00
7	Pad	25# Hybor	60.0	60	10000	74000	10000		3400	203		
8	0.50 ppg Premium White 30/50	25# Hybor	68.4	70	15000	89000	15342	75	3325	278	0.50	0.50
9	1.00 ppg Premium White 30/50	25# Hybor	66.9	70	15000	104000	15684	150	3175	428	1.00	1.00
10	1.25 ppg Premium White 30/50	25# Hybor	66.2	70	20000	124000	21140	250	2925	678	1.25	1.25
11	1.50 ppg Premium White 30/50	25# Hybor	65.5	70	20000	144000	21368	300	2625	978	1.50	1.50
12	1.75 ppg Premium White 30/50	25# Hybor	64.8	70	20000	164000	21596	350	2275	1328	1.75	1.75
13	2.00 ppg Premium White 30/50	25# Hybor	64.1	70	25000	189000	27280	500	1775	1828	2.00	2.00
14	2.50 ppg Premium White 30/50	25# Hybor	62.8	70	20000	209000	22280	500	1275	2328	2.50	2.50
15	2.50 ppg Premium White 20/40	25# Hybor	62.8	70	19000	228000	21166	475	800	2803	2.50	2.50
16	3.00 ppg Premium White 20/40	25# Hybor	61.6	70	15000	243000	17052	450	350	3253	3.00	3.00
17	3.50 ppg Premium White 20/40	25# Hybor	60.4	70	10000	253000	11596	350	0	3603	3.50	3.50
	Totals:					253,000	269,427	3,603				

The pumping schedule for a liquid hydrocarbon well in the Eagle Ford Shale near Runge, Texas performed in March 2014.

APPENDIX E

Number	Stage Desc.	(bbls)	Proppant Conc. (Lbm / gal) Start	End	Density (Lbm / gal)	Volume (gallons)	Dirty Volume (gallons)	Slurry Rate (bpm)	Time each Stage (minutes)	Sacks (used)	Sacks per min. (remaining)
Treated Water		3848				161595	170715		83		2000
Stage 1	Breakdown				8.33	**12000**	12000	15	19.0		
15% HCl		3562				149595	158715		64		2000
Stage 2	Acid				8.33	**1500**	1500	20	1.8		
Treated Water		3526				148095	157215		62		2000
Stage 3	Displacement				8.33	**45000**	45000	60	17.9		
Water Frac G 25#		2455				103095	112215		45		2000
Stage 4	Pre-Pad				8.33	**5000**	5000	60	2.0		
Hybor G 25#		2336				98095	107215		43		2000
Stage 5	Pad				8.33	**10000**	10000	60	4.0		
Hybor G 25#		2098	30/50 Ottawa		0.0456	88095	97215		39		2000
Stage 6	1 PPG SLF		1.00	1.00	8.92	**10000**	10456	60	4.1	100	24.1
Hybor G 25#		1859	30/50 Ottawa		0.0456	78095	86759		34	100	1900
Stage 7	2 PPG SLF		2.00	2.00	9.47	**15000**	16368	60	6.5	300	46.2
Hybor G 25#		1502	30/50 Ottawa		0.0456	63095	70391		28	400	1600
Stage 8	3 PPG SLF		3.00	3.00	9.97	**20000**	22736	60	9.0	600	66.5
Hybor G 25#		1026	30/50 Ottawa		0.0456	43095	47655		19	1000	1000
Stage 9	4 PPG SLF		4.00	4.00	10.43	**25000**	29560	60	11.7	1000	85.3
Treated Water		431				18095	18095		7	2000	
Stage 10	Flush				8.33	**18095**	18095	60	7.2		
						0.0	0.0		0.0	2000	0.0

Treatment Info: ***SO#*** ***901142719***

Total Time:	83	min
Expected Frac Gradient:	0.93	psi/ft
Expected Treating Pressure:	8,000	psi
Expected HHp:		HHp
Expected BHTP:	16,648	psi
Pipe Time:	#DIV/0!	min
BHST:	260	°F
Pad Percentage	11.8	%

Wellbore Info:

Top Perf:	17,825	ft.
Volume to Bottom Perf	15,995	gal
Mid Perf TVD:	17,901	ft.

Prop & Fluids Info:

PROPPANT		
30/50 Ottawa =	**2000**	100*lbm
Total Proppant=	**2000**	100*lbm

FLUIDS		
Treated Water	**75095**	gal
Water Frac G 25#	**5000**	gal
Hybor G 25#	**80000**	gal

The pumping schedule for a liquid hydrocarbon well in the Eagle Ford Shale near Kennedy, Texas performed in April 2014.